Institute of Physics, Polish Academy of Sciences

Advancing Accurate Composition Analysis of Ternary Semiconductors: Matrix Effects in Secondary Ion Mass Spectrometry

Zeinab Khosravizadeh

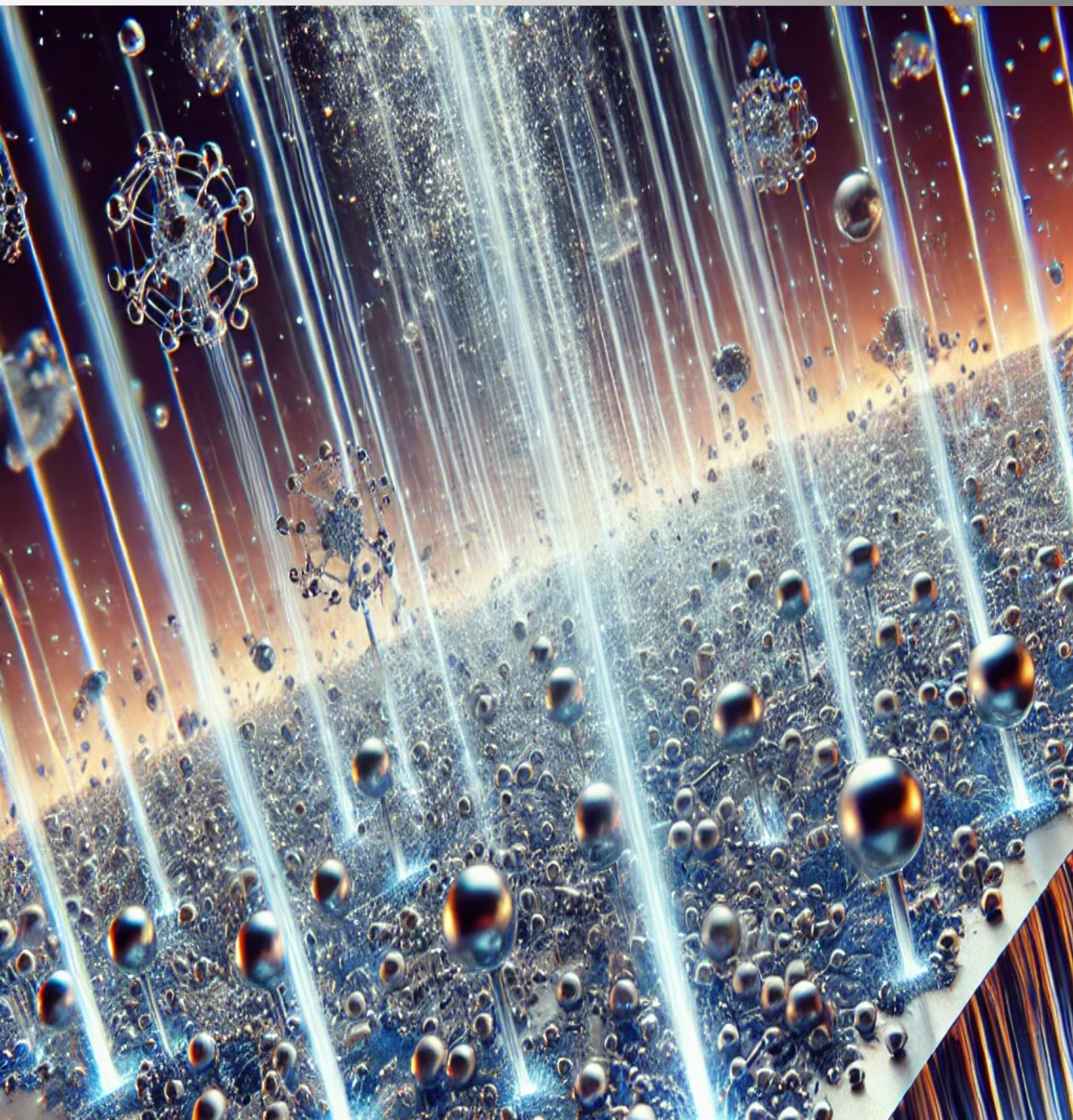

Institute of Physics, Polish Academy of Sciences

Advancing Accurate Composition Analysis of Ternary Semiconductors: Matrix Effects in Secondary Ion Mass Spectrometry

Zeinab Khosravizadeh

A thesis submitted in fulfillment of the requirements
for the degree of Doctor of Philosophy in Physics

13 December 2024

PhD thesis at Polish Academy of Science
Report no. IFPAN-2024-12

Supervisor:

Dr hab. Rafał Jakieła, Prof. IFPAN

Published and Distributed by
Polish Academy of Science
Department of Physics
Division of X-ray and Electron Microscopy Research
X-ray spectroscopy and microanalysis Group
Al. Lotników 32/46, 02-668, Warszawa, Poland
Tel: (+48 22) 843 70 01
www.ifpan.edu.pl

Printed in Poland
13 December 2024

The image on the front cover is generated by AI.

Declaration

I hereby declare that this thesis, titled *"Advancing Accurate Composition Analysis of Ternary Semiconductors: Matrix Effects in Secondary Ion Mass Spectrometry,"* is my original research and has not been submitted for any other degree or qualification at this or any other institution. This thesis is submitted to fulfill the requirements for the Doctor of Philosophy degree at the Institute of Physics, Polish Academy of Sciences.

Zeinab Khosravizadeh
13 December 2024

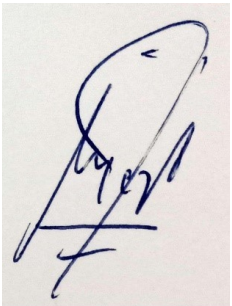

Abstract

Ternary compound materials are gaining substantial attention with the development of semiconductor technology. Owing to their comprehensive applications, precisely quantifying the matrix composition of ternary compounds has become increasingly vital. In this context, surface analysis techniques are crucial to facilitating accurate characterization for advancing material science. Applying secondary ion mass spectrometry (SIMS) is challenging among these techniques due to the impact of the matrix effect. The matrix elements in a material influence the secondary ions ejected from the surface, causing variations in ionization yield with the compound's composition. The matrix effect is related to changes in the material's electronic properties, such as work function.

This study investigates matrix effects in the SIMS analysis of ternary compound semiconductors. To assess how matrix composition influences secondary ion yield and the accuracy of composition determination. The thesis is divided into two main sections: the first part focuses on matrix effects in the $Cd_{1-x}Zn_xO$ ternary compound, while the second explores matrix effects in $Pb_{1-x}Sn_xTe$.

$Cd_{1-x}Zn_xO$ ($0 < x < 0.6$), a widely used ternary compound semiconductor popular mostly in optoelectronic applications, and $Pb_{1-x}Sn_xTe$ ($0 < x < 1$) another applicable ternary compound demonstrates non-linearity in band structure near critical composition points, making it an ideal candidate for studying the matrix effect. It should be noted that while the matrix effect complicates the quantitative analysis of the material composition, it concurrently allows for valuable inference about the electronic and chemical properties of the studied semiconductor.

A contribution of this research is the development of a calibration curve method using SIMS to determine the composition of CdZnO and PbSnTe ternary compounds accurately. With the use of these calibration curves, we can accurately measure the elemental composition of $Cd_{1-x}Zn_xO$ and $Pb_{1-x}Sn_xTe$ in any structure, which is difficult to achieve with other methods. An innovative aspect of this study is introducing a new approach for SIMS instruments, allowing for estimating the band gap behavior of ternary compound semiconductors of $Pb_{1-x}Sn_xTe$ for the first time while accounting for the matrix effect in SIMS analysis.

This study advances the understanding of matrix effects in SIMS analysis, which is crucial for improving the accuracy of material characterization. Ultimately, the research aims to develop more accurate and reliable analytical methods, supporting fundamental research and practical applications in the semiconductor industry.

Streszczenie

Wraz z rozwojem technologii półprzewodników, materiały trójskładnikowe zyskują coraz większą uwagę. Ze względu na ich szerokie możliwości zastosowań, precyzyjne określenie składu matrycy związków ternarnych staje się coraz bardziej istotne. W tym kontekście, techniki analizy powierzchni umożliwiające dokładną charakteryzację zaawansowanych materiałów, odgrywają kluczową rolę w rozwoju nauki na ich temat. Spośród technik, spektrometria masowa jonów wtórnych (SIMS) jest jedną z najbardiej zaawansowanych technik pomiarowych. Jednak jej wykorzystanie związane jest z trudnością wynikającą z tzw. efektu matrycowego. Efekt ten wynika stąd, że pierwiastki znajdujące się w materiale wpływają na wydajność jonizacji atomów, które sa analizowane podczas pomiaru. Efekt matrycy jest głównie związany ze zmianami właściwości elektronicznych materiału, takimi jak praca wyjścia i powinowactwo elektronowe.

Niniejsza praca poświęcona jest badaniom wpływu efektu matrycy na analizę składu trójskładnikowych związków półprzewodnikowych metodą SIMS. Celem jest ocena, jak skład matrycy wpływa na wydajność jonów wtórnych oraz dokładność identyfikacji składu materiału. Praca podzielona jest na dwie główne części. Pierwsza z nich koncentruje się na efektach matrycy w trójskładnikowym związku takim jak tlenek cynkowo-kadmowy $Cd_{1-x}Zn_xO$ natomiast druga analizuje efekt matrycy w tellurku ołowiowo-cynowym $Pb_{1-x}Sn_xTe$. Zarówno $Cd_{1-x}Zn_xO$ półprzewodnik szeroko stosowany głównie w zastosowaniach optoelektronicznych jak i $Pb_{1-x}Sn_xTe$ wykazujący potencjalne możliwości aplikacyjne, charakteryzujący się nieliniowością struktury pasmowej w pobliżu punktów krytycznych składu, są idealnymi kandydatami do badania efektu matrycy w metodzie SIMS.

Nowatorskim aspektem niniejszego badania było opracowanie metody krzywych kalibracyjnych w badaniach SIMS do określenia dokładnej zawartości związków trójskładnikowych. Zastosowanie jej umożliwia precyzyjne określenie składu pierwiastkowego $Cd_{1-x}Zn_xO$ oraz $Pb_{1-x}Sn_xTe$ w dowolnej strukturze półprzewodnikowej, co jest trudne do osiągnięcia innymi metodami pomiarowymi.Dodatkowo, innowacyjny aspekt tych badań polega na wprowadzeniu nowego podejścia do pomiarów metodą SIMS, które pozwalają na obserwację zmian przerwy energetycznej $Pb_{1-x}Sn_xTe$ z wykorzystaniem efektu matrycy. Niniejsze badania pogłębiają zrozumienie efektów matrycy w analizie SIMS, co jest kluczowe dla poprawy dokładności charakterystyki materiałów. Ostatecznie, ce-

lem badań jest opracowanie bardziej precyzyjnych i niezawodnych metod analitycznych, wspierających zarówno badania podstawowe jak i praktyczne zastosowania w przemyśle półprzewodników.

نه تو می مانی و نه اندوه،

و نه هیچ یک از مردم این آبادی!
به حباب نگران لب یک رود قسم،
و به کوتاهی آن لحظه ی شادی که گذشت،
غصه هم می گذرد!
آنچنانی که فقط خاطره ای خواهد ماند،
لحظه ها عریانند.
به تن لحظه خود، جامه اندوه مپوشان هرگز...
(سهراب سپهری)

Neither you remain, nor sadness,

And not any of the people of this village!
Swear to the anxious bubble on the edge of a river,
And to the brevity of that moment of joy that passed,
Sadness will also pass!
Just as it will remain only a memory,
Moments are pristine.
Do not ever dress the moment in the garment of sorrow…
(*Sohrab Sepehri*)

Translated by Zeinab Khosravizadeh

Acknowledgments

I would like to express my heartfelt gratitude to my supervisor, Dr. hab. Rafał Jakieła, Prof. IFPAN, for his unwavering support throughout this journey. With deep admiration, I appreciate his patience and compassionate guidance, without which I would not have been able to accomplish this work. I feel incredibly fortunate to have had such a dedicated and caring mentor. I am also thankful to Prof. Barcz for his invaluable review of my thesis. I sincerely thank Julita for her kindness and assistance translating the abstract into Polish. To Adrian, I am profoundly grateful for your steadfast guidance, constant encouragement, and invaluable support throughout this work. Your insightful advice has been a source of strength in completing this research.

To my extraordinary parents, Ali and Fatemeh, your love, patience, kindness, wisdom, belief, and hope were the first lessons I learned from you. I am beyond blessed to have you in my life, and I love you more than words can express. To my wonderful siblings—Hosein, Bahar, Mojtaba, Mohsen, and Zahra— my grandparents, all my brothers-in-law and sisters-in-law, and my dear nephews, Amir Ali and Ava: thank you for your open arms and endless love from afar. Your support and kindness have been invaluable during this exploration. You are always in my heart.

سپاس خدای را که هر چه دارم از اوست،
و قدردان پدر و مادر عزیزم ،
آن گوهرهای نابی که !
با عشق بی‌پایان و حمایت بی‌دریغشان،
پشتوانه و چراغ راه من بوده اند،
سپاسگزار و دست‌بوس
مهر بی کران تان هستم.

از پدربزرگ و مادربزرگم،
که خاطرات شان،
روشنایی‌بخش راه زندگی‌ام بوده.
از خواهران و برادرانم،
که زندگی بی عشق و حضور پرمهرشان ،
معنایی نداشت...
و دوستانم،
که صفای وجودشان
پشتیبان لحظات سخت زندگی‌ام بود.

Dedication

To my beloved parents—your boundless love, faith, support, and countless sacrifices have made every step of this journey possible. This achievement is a reflection of the dreams you helped me believe in.

Research Articles

This thesis is based on the results published in articles incorporated into this study.

Paper I

- Khosravizadeh, Z., Trzyna-Sowa, M., Lysak, A., Przeździecka, E., Jakiela, R., "Accurate determination of matrix composition in $Cd_{1-x}Zn_xO$ semiconductor material using MS-SIMS and ToF-SIMS methods," Journal of Physics D: Applied Physics, 58 (2024) 025303, http://iopscience.iop.org/article/10.1088/1361-6463/ad80a0.

Paper II

- Khosravizadeh, Z., Dziawa, P., Dad, S., Jakiela, R., "Secondary Ion Mass Spectrometry Characterization of Matrix Composition in Topological Crystalline Insulator $Pb_{1-x}Sn_xTe$," Thin Solid Films, 781 (2023) 139974, https://doi.org/10.1016/j.tsf.2023.139974.

Paper III

- Khosravizadeh, Z., Dziawa, P., Dad, S., Dabrowski, A., Jakiela, R., "A novel approach for observing band gap crossings using the SIMS technique in $Pb_{1-x}Sn_xTe$," Journal of Semiconductors, 45 (2024) 112102, https://www.jos.ac.cn/en/article/doi/10.1088/1674-4926/24040023.

Additional Publications During Ph.D.

1. **Khosravizadeh Z.**, Lysak A., Przeździecka E., Jakieła R., " SIMS and Numerical Analysis of Asymmetrical Out-Diffusion of Hydrogen and Carbon in $Cd_{1-x}Zn_xO$ Multilayer," Materials, 17 (2024) 5240, https://doi.org/10.3390/ma17215240

2. Obrębowski, Sz., Ćwik, K., Srivatsa, Sh., Uhl, T., Jagielski, J., Wolska, A., Klepka, M., **Khosravizadeh, Z.**, Jakieła, R., Trzyna-Sowa, M., Wojciechowski, T., Szwacki, N.G., Marynowski, W., Lewiński, J., Zybała, R., Borysiewicz, M.A., "Ion implanted MXene electrodes for selective VOC sensors," Applied Materials Today, 39 (2024) 102343, https://doi.org/10.1016/j.apmt.2024.102343

3. Przeździecka, E., Lysak, A., Adhikari, A., Stachowicz, M., Wierzbicka, A., Jakiela, R., **Khosravizadeh, Z.**, Sybilski, P., Kozanecki, A., "Influence of the growth temperature and annealing on the optical properties of CdO/ZnO30 superlattices," Journal of Luminescence, 269 (2024) 120481, https://doi.org/10.1016/j.jlumin.2024.120481

4. Lysak, A., Przeździecka, E., Wierzbicka, A., Jakiela, R., **Khosravizadeh, Z.**, Szot, M., Adhikari, A., Kozanecki, A., "Temperature Dependence of the Bandgap of Eu-Doped ZnCdO/ZnO30 Multilayer Structures," Thin Solid Films, 781 (2023) 139982, https://doi.org/10.1016/j.tsf.2023.139982.

5. Bermejo-Ortiz, J., Krizman, G., Jakiela, R., **Khosravizadeh, Z.**, Hajlaoui, M., Bauer, G., Springholz, G., de Vaulchier, L.-A., Guldner, Y., "Observation of Weyl and Dirac Fermions at Smooth Topological Volkov-Pankratov Heterojunctions," Phys. Rev. B, 107 (2023) 075129, https://doi.org/10.1103/PhysRevB.107.075129.

6. Mishra, S., Witkowski, B.S., Jakiela, R., **Khosravizadeh, Z.**, Paszkowicz, W., Sulich, A., Volnianska, O., Wozniak, W., Guziewicz, E., "Cathodoluminescent Imaging of ZnO:N Films: Study of Annealing Processes Leading to Enhanced Acceptor Luminescence," Phys. Status Solidi A, 220 (2023) 2200466, https://doi.org/10.1002/pssa.202200466.

7. Lysak, A., Przeździecka, E., Wierzbicka, A., Jakiela, R., Reszka, A., Witkowski, B., **Khosravizadeh, Z.**, Adhikari, A., Sajkowski, J.M., Kozanecki, A., "Effect of Rapid Thermal Annealing on Short Period CdO/ZnO Multilayer Structures Grown on m-Al2O3," Mater. Sci. Semicond. Process., 142 (2022) 106493, https://doi.org/10.1016/j.mssp.2022.106493.

8. Gas, K., Królicka, A., Dybko, K., Nowicki, P., **Khosravizadeh, Z.**, Story, T., Sawicki, M., "Magnetic Constitution of Topologically Trivial Thermoelectric PbTe: Cr," Journal of Magnetism and Magnetic Materials, 537 (2021) 168154, https://doi.org/10.1016/j.jmmm.2021.168154.

Conference Publications During Ph.D.

1. Gorlin, M., Saguì, N.A., Zheng, D.J., McCormack, K.L., **Khosravizadeh, Z.**, Kim, J., Xu, H., Peng, J., Malmberg, P., Román-Leshkov, y., Valvo, M., Shao-Horn, y., Edvinsson, T., "Lattice Oxygen Exchange in Transition Metal Oxyhydroxides and Metal Hydroxide Organic Frameworks Elucidated for the Oxygen Evolution Reaction," ECS Meeting Abstracts, MA2023-02 (2023) 2146, https://dx.doi.org/10.1149/MA2023-02422146mtgabs

Contents

List of Figures

List of Tables

List of Acronyms

- Secondary Ion Mass Spectrometry (SIMS)
- Magnetic Sector Secondary Ion Mass Spectrometry (MS-SIMS)
- Time of Flight Secondary Ion Mass Spectrometry (ToF-SIMS)
- Relative Sensitivity Factor (RSF)
- Reflection High-Energy Electron Diffraction (RHEED)
- Molecular Beam Epitaxy (MBE)
- Parts Per Million (ppm)
- Parts Per Billion (ppb)
- Quadrupole Mass Analyzers (QMA)
- Radio Frequency (RF)
- Standard Cubic Centimeters Per Minute (sccm)
- Direct Current (DC)
- Faraday Cups (FC)
- Electron Multipliers (EM)
- Resistive Anode Encoder (RAE)
- Sputtering Rate (SR)
- X-ray diffraction (XRD)
- Energy-Dispersive X-ray (EDX)
- Scanning Electron Microscope (SEM)
- Light-Emitting Diodes (LEDs),
- Conduction Band Minimum (CBM)
- Valence Band Maximum (VBM)
- Ultraviolet (UV)
- Adopted from (adopt. from)

Chapter 1

Introduction

1.1 Surface Characterization Techniques

Advances in materials science, particularly in the semiconductor industry, heavily depend on accurate surface characterization techniques. These methods are critical for understanding the structural, chemical, and physical properties of materials, enabling the design and optimization of new technologies in fields such as optoelectronics, photovoltaics, and thermoelectrics [1–3].

Surface analysis techniques involve directing primary beams of electrons, ions, X-rays, or photons onto a material's surface, generating signals from ejected particles such as ions, photons, and electrons. These signals are analyzed to determine the material's surface properties [4]. Among the many available techniques, secondary ion mass spectrometry (SIMS) stands out for its exceptional sensitivity and versatility [5, 6].

SIMS is a powerful technique for surface analysis, capable of providing precise elemental and isotopic composition data. With detection limits as low as parts per billion, SIMS enables unparalleled insights into material structures and compositions. Its ability to analyze complex materials makes it indispensable in semiconductor research, particularly for emerging materials like ternary semiconductors, where precise control of elemental composition is critical [5, 7, 8].

1.2 Challenges in SIMS Analysis

Despite its strengths, SIMS faces significant challenges in achieving accurate elemental quantification for ternary semiconductors. One of the most critical issues is the occurrence of matrix effects—phenomena where the chemical environment influences ionization efficiencies, distorting secondary ion yields and introducing inaccuracies in quantification [9].

Ternary compound semiconductors, composed of three distinct elements, are particularly interesting for their unique properties and applications in advanced technologies. Materials such as cadmium zinc oxide ($Cd_{1-x}Zn_xO$) [10–12] and lead tin telluride ($Pb_{1-x}Sn_xTe$) [13–18], exemplify these challenges. Their complex compositions and chemical interactions result in significant variations in ionization behavior, complicating SIMS analysis. Accurate elemental characterization of these materials is essential, as

even minor deviations in composition can have substantial impacts on their electrical and optical performance.

Beyond compositional challenges, the behavior of electronic properties plays a critical role in how matrix effects manifest during SIMS measurements. Addressing these interconnected challenges is essential for understanding the mechanisms behind matrix effects in SIMS analysis of ternary semiconductors.

1.3 Practical Challenges of Matrix Effects

Matrix effects in SIMS arise due to the high sensitivity of sputtering and ionization processes to the local chemical and physical environment of the sample. The presence of certain elements can enhance or suppress the ionization of others, resulting in nonlinear relationships between secondary ion intensities and the actual elemental concentrations [9]. Such nonlinearities complicate accurate quantification, particularly in ternary semiconductors, where variations in elemental ratios, chemical bonding, and electronic properties exacerbate matrix effects and necessitate advanced calibration techniques.

For example, changes in the ratio of constituent elements in materials like CdZnO and PbSnTe can significantly alter ionization yields, distorting SIMS signals and introducing systematic errors. Additionally, compositional gradients and heterogeneities, such as stoichiometric variations, further complicate data interpretation. Addressing these challenges requires unique calibration curves to account for each specific system. While existing studies have been developed for simpler systems, such as AlGaAs [19], InGaAsP [20], and HgCdTe [21], calibration methods for ternary semiconductors remain not fully understood.

Furthermore, electronic properties, such as work function and electron affinity, influence the probability of the secondary ion emission and contribute to variations in the measured SIMS signal. Understanding the interplay between electronic properties and matrix effects is essential for improving both the theoretical understanding and practical applications of SIMS to explore fundamental material behaviors.

1.4 Goals and Scope

This research is driven by the increasing demand for accurate material characterization techniques to advance semiconductor technology. Specifically, this study focuses on understanding and mitigating matrix effects in SIMS analysis of ternary semiconductors, emphasizing improving quantification accuracy and exploring the impact of electronic properties on ionization behavior.

The scope of this research encompasses two main goals: Developing improved calibration methods to enhance the accuracy of elemental quantification in ternary semiconductors. Furthermore, investigating the role of electronic properties in matrix effects, specifically exploring their influence in altering ionization probabilities during SIMS analysis.

CdZnO and PbSnTe are selected as model systems due to their significant technological relevance and complex compositional challenges. The insights gained from this study are expected to advance the understanding of matrix effects and contribute to developing more accurate SIMS methodologies for complex materials. Moreover, utilizing SIMS to explore how electronic properties contribute to these matrix effects provides a fresh perspective, expanding its role as an analytical tool and revealing new potential applications for SIMS. Ultimately, this research aims to offer practical solutions that can advance research on semiconductor materials and technology.

1.5 Research Objectives

The primary objective of this research is to improve the accuracy and reliability of SIMS as an analytical tool to address a key challenge in semiconductor research. Moreover, the role of electronic properties in the matrix effects in the ternary compound semiconductor in SIMS analysis is explored. The specific objectives of this research are:

Research Question 1: How do matrix effects impact SIMS measurement accuracy?
Matrix effects can significantly alter secondary ion yields, affecting the accuracy of SIMS measurements. This objective focuses on the relationship between matrix effects and ionization yields to improve the reliability of compositional analysis.

Research Question 2: How can we overcome matrix effects for precise quantification in SIMS?
This objective aims to develop calibration techniques specifically tailored to ternary systems, which are crucial for achieving precise quantification. The goal is to construct robust calibration curves, particularly for materials like CdZnO and PbSnTe.

Research Question 3: What is the role of electronic properties of ternary semiconductors in matrix effects?
This objective investigates how the electronic properties of PbSnTe contribute to variations in ionization probability behavior. Understanding these mechanisms will provide deeper insights into matrix effects and inform improved analytical strategies. This is a novel application of SIMS for this category of materials.

1.6 Limitations

While this study provides valuable insights into the quantification of ternary semiconductors using SIMS and the impact of electronic properties on matrix effects, certain limitations must be acknowledged:

- Calibration Curve Specificity: The calibration curve developed in this study is unique to the specific ternary compounds studied (CdZnO and PbSnTe). While this curve offers improved accuracy for these materials, its applicability to other ternary systems may be limited. Each ternary compound may require its own calibration curve due to variations in ionization behaviors and matrix effects. Therefore, while tailored to the materials discussed, this work provides a universal calibration method.
- Electronic Properties Measurement Limitation: In studying the electronic properties of PbSnTe compounds, the resolution of energy distribution has a limitation of about 0.16 eV. This limited the precision with which we could measure and analyze variations in the electronic properties of the materials, like work function and electron affinity.

1.7 Outline

The structure of this thesis is divided into the following:

- **Chapter 2: SIMS and Matrix Effects** – This chapter includes literature and reviews on SIMS, how it works, details of understanding of ionization phenomena, and most importantly, the matrix effects in the SIMS method and the theory behind our works.
- **Chapter 3: Materials and Measurements** – This chapter outlines the reviews on ternary compound semiconductors, a brief overview of CdZnO and PbSnTe, and experimental procedures such as sample growth, SIMS measurement conditions, and data analysis techniques.
- **Chapter 4: Results: Summary of Publications** – In this chapter, a summary of the results of each paper is presented, followed by the attached papers incorporated in this study at the end of this chapter.
- **Chapter 5: Conclusions and Outlook** – At the end, there is a summary of our works in this chapter, including the response to the research questions, the general conclusions in this study, and suggestions for future potential work in this field.

Chapter 2

SIMS and Matrix Effects

2.1 Overview of SIMS

Secondary ion mass spectrometry is an analytical technique used to estimate the composition in solid surfaces and near-surface layers (up to tens of micrometers) based on the sputtering process [5]. The history of SIMS dates back to 1910 when Thomson observed radiation of secondary ions from a metallic surface [22]. Later, he discovered the ratio of charge to mass of ions (e/m) by passing through a magnetic field in vacuum tubes.

In 1949, Herzorg and Viehboeckthe reported the prototype of the SIMS instrument using an improved canal-ray tube, incorporating two electric fields, and conducting sputtering in a high vacuum environment [23]. Eventually, the first commercial SIMS instrument was released by Herzog under a NASA project in 1967, aimed at detecting and analyzing mineral materials discovered during space missions [24]. Raimond Castaing and his Ph.D. student, Slodzian, at the University of Paris-Sud in France, developed a dynamic SIMS device based on magnetic sector mass spectrometry, utilizing argon as the primary beam for bombarding samples [5].

Despite fulfillment in applying mass spectrometry for gaseous samples, it encountered technical challenges related to vaporization and ionization during that period for solids analysis [24]. With the growing need to characterize the surface properties of thin films by developing the industry, SIMS gained significant attention due to its ability to detect all elements in the periodic table. Its high sensitivity, ranging from parts per million (ppm) to parts per billion (ppb), along with nanometer-scale depth resolution and isotopic separation, makes it superior to other surface analysis techniques [7, 25–28]. This advancement led to the widespread application of SIMS across various fields, as reviewed by Williams in 1985 [29], followed by Vleck and later by Bacon et al. [30, 31].

2.2 Basics of SIMS

Mass spectrometry generates ions from compounds through various methods, such as thermal ionization, electric fields, or impacts from energetic electrons, ions, or photons. In SIMS, the surface of a sample is bombarded with accelerated ions known as primary beams. When the primary beam collides with the sample surface, it transfers sufficient energy to eject atoms from the surface into the vacuum. These sputtered particles can

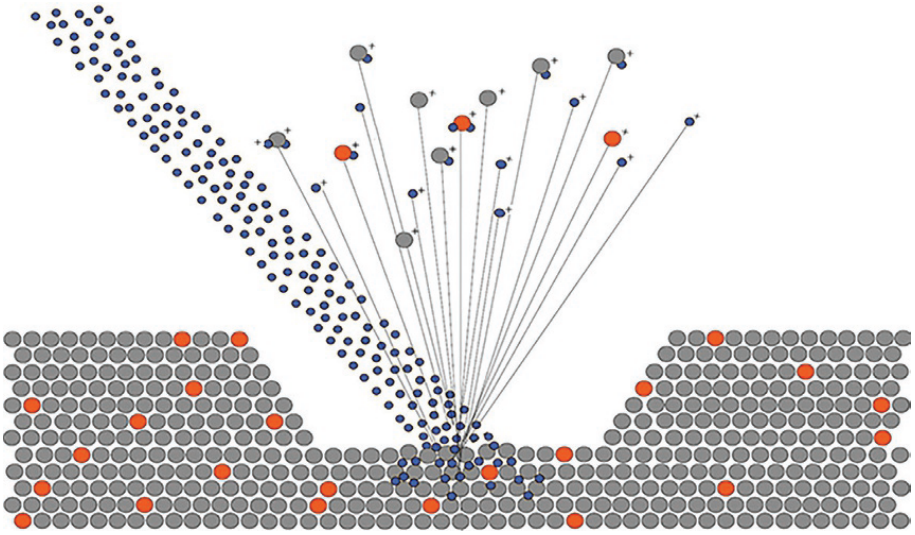

Figure 2.1: Schematically representation of sputtering of secondary ions and ionization yields by the primary beam (Taken from [5]).

include electrons, neutral atoms, molecules, and positively and negatively charged ions (order of 0.1–10%), referred to as secondary ions. Figure 2.1 (Adopt. from [5]) schematically illustrates the sputtering of the secondary ions from the surface. The potential difference between the sample and the detector accelerates the secondary ions into a mass spectrometer, which is analyzed by energy and mass using electric and magnetic fields. After mass analysis, the secondary ions are collected by detectors.

SIMS operates in two main modes: static and dynamic [5]. In the static mode, which is non-destructive under specific bombardment conditions, the low-dose energy primary beam results in the ejection of secondary ions from the surface's top layer. Static SIMS can give information about the surface composition [8]. On the other hand, dynamic SIMS operates by applying high-dose primary beams to the deeper beneath-the-surface analysis. The removed material in the analyzed region enables depth profiles, mass spectra, the image of the surface, and depth-resolved images [32].

A typical SIMS device comprises four primary components: a primary ion source, an energy analyzer, a mass analyzer, and a detector, all functioning within high vacuum conditions. A schematic representation of SIMS components is shown in Figure 2.2 (Adopt. from [32]).

2.2.1 Primary Ion Source

The ion source is crucial for generating the ions (primary beam) that bombard the surface of the sample, causing the ejection of secondary ions for analysis (see Figure 2.3, adopt. from [32]). The primary beam contains ions of elements like cesium, oxygen, or argon

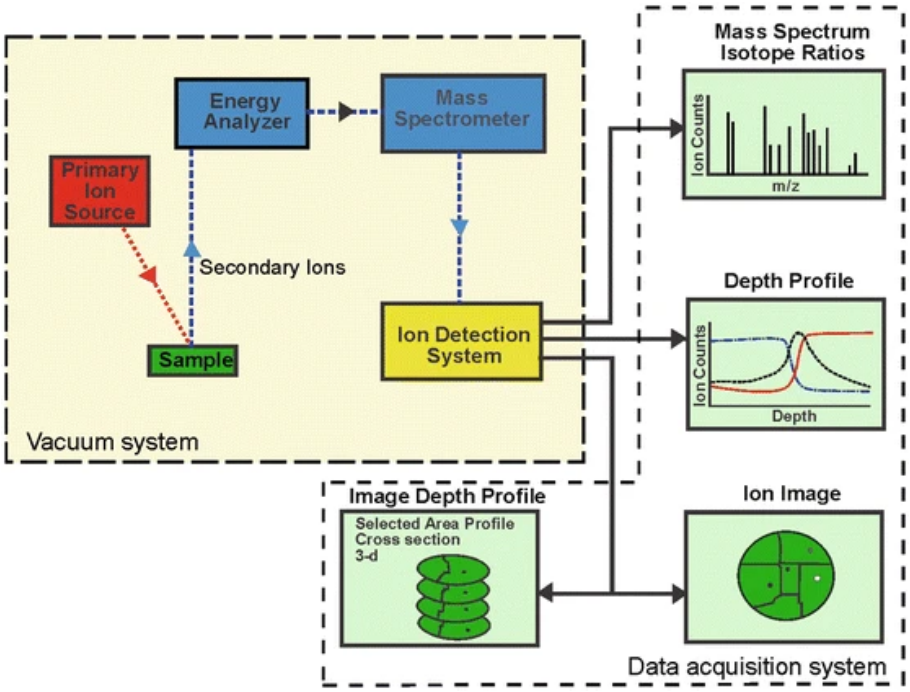

Figure 2.2: Schematically representation of SIMS instruments (Taken from [32]).

(Cs^+, O_2^+, O^-, Ar^+, Xe^+, Ga^+, etc.) and is accelerated at high energies (often up to 25 keV) toward the sample. The choice of ion type depends on the desired effect: oxygen ions (O_2^+) are commonly used to enhance the emission of positively charged secondary ions like Al, B, etc., while cesium ions (Cs^+) are more effective for negative ion production like C, O, etc. The focused ion beam can target specific sample areas, enabling lateral resolution analysis. The properties of the primary ion beam, such as energy, type, and spatial resolution, directly influence the sputtering process and the depth profiling capabilities of the SIMS instrument [32].

2.2.2 Energy Analyzers

In the sputtering process, secondary ions ejected from a surface have a wide range of energies. The secondary ions enter the electrostatic energy analyzer, ensuring that only ions with a specific energy (and constant velocity) can pass through. After that, a movable energy slit is positioned to selectively filter a narrow range of the dispersed secondary ions, allowing only a chosen fraction with the proper range of energy to pass through the magnetic analyzer. The energy distribution of molecular ions is much narrower than atomic ions. An energy slit at the output of the electrostatic analyzer can intercept the ions with the required energy, allowing them to continue through the mass spectrometer (see Figure 2.4, adopt. from [33]).

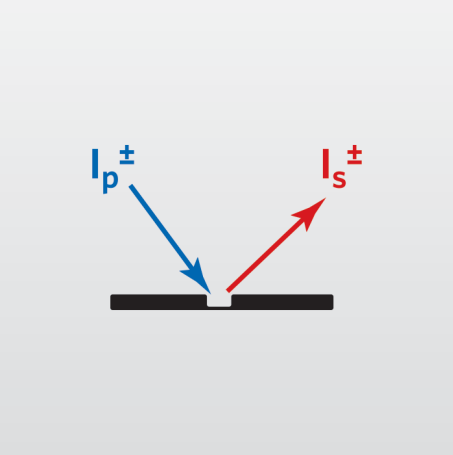

Figure 2.3: Schematically representation of primary ion (I_p) and secondary ion (I_s) on the surface (Taken from [32]).

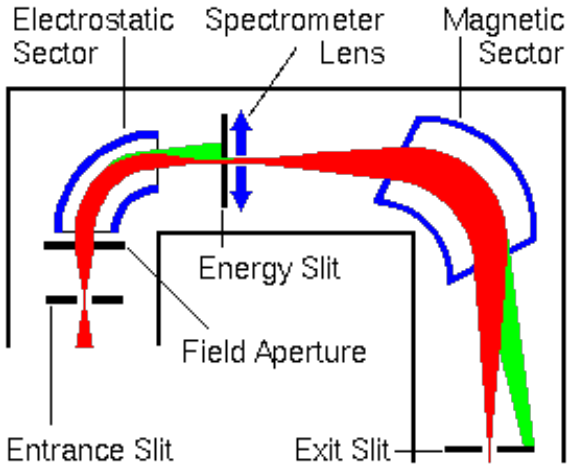

Figure 2.4: Schematically representation of the energy and mass analyzers in SIMS device (Taken from [33]).

2.2.3 Mass Analyzers

There are three types of mass analyzers in SIMS: a magnetic sector (MS), time-of-flight (ToF), and quadrupole mass analyzer (QMA). Two essential factors for comparing mass analysis are mass resolution and transmission [32]. The ability of the mass analyzer to distinguish among distinct mass-to-charge ratios is called mass resolution. This resolution can be determined by dividing the mass of the first peak (m) or the average mass of two peaks by the difference in mass between two peaks (δm). This is mathematically expressed as R = m/ δm, where R represents the resolution. Moreover, the percentage of ions that can pass through a specific area of the mass spectrometer refers to the transmission, which can be estimated by comparing exiting and entering ions on that region [32].

2.2.3.1 Magnetic Sector SIMS Analyzer

The MS-SIMS analyzer applies a magnetic field to separate charged particles according to their mass-to-charge ratio. The physics behind this phenomenon- how charged particles move through a constant magnetic field- can be described by the Lorentz force law, which is the force applied to a charged particle moving through the magnetic field. The Lorentz force (F_L) depends on the velocity (v), the intensity of the magnetic field (B), and the charge of the ion (q). The Lorentz force is given by:

$$\mathrm{F}_L = qvB\sin\alpha \tag{2.1}$$

F_L can be equal to qvB, if the v and B are perpendicular. On the other hand, from a centripetal force (F_c), when a charged particle is moving into the uniform magnetic field, it is drawing a circular path with the radius (r_m). The following expression describes the F_c:

$$F_c = \frac{mv^2}{r_m} \tag{2.2}$$

The equivalence between the centripetal force (2.2) and the Lorentz force (2.1) gives us:

$$qvB = \frac{mv^2}{r_m} \tag{2.3}$$

where the mass-to-charge ratio can be expressed as:

$$\frac{m}{q} = \frac{Br_m}{v} \tag{2.4}$$

- $\frac{m}{q}$ is the mass-to-charge ratio ($\frac{\mathrm{kg}}{\mathrm{C}}$), it changes into $\frac{m}{z}$, z is the number of ion's charges concerning the elementary charge),
- B is the strength of the magnetic field ($\frac{\mathrm{Wb}}{\mathrm{m}^2}$),
- v is the velocity ($\frac{\mathrm{m}}{\mathrm{s}}$),
- r is the radius of the ion trajectory in the magnetic field (m).

By adjusting the apertures and slits in the secondary ion beam path, high transmission (up to 20%) and mass resolution (up to 25,000) can be attained. The primary features of the SIMS system are extremely shallow or deep depth profiling and low detection limit of elements.

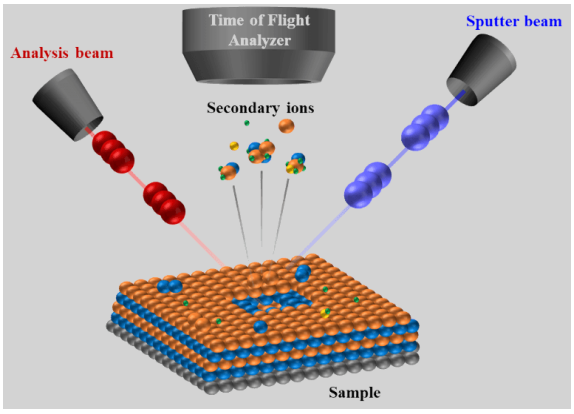

Figure 2.5: Schematically representation of the duel beam ToF-SIMS device (Taken from [34]).

2.2.3.2 Time of Flight SIMS Analyzers

ToF-SIMS employs a pulsed primary ion beam, typically Cs or Bi (other sources like Ga, Ar, Xe, SF5, and C60), to selectively remove material from the surface for analyzing and characterizing the surface content. ToF-SIMS operates using a dual-beam system: both ion beams are used to sputter the material, but only ions ejected by the second beam are analyzed (see Figure 2.5, adopt. from [34]).

Upon bombarding the surface with primary ions, species are ejected from the atomic monolayer and accelerated through a flight tube. The masses of species are determined based on their flight times to reach the detector from the initiation of the pulse. Heavier species require more time to reach the detector. ToF-SIMS is designed with a circular path (a reflectron) to increase the flight path and enhance resolution by extending the time difference between masses.

This instrument can gain high transmission (from 10 in the case of inorganic ions, up to 90% for organic ions) and mass resolution (up to 10,000). The high transmission and mass range detection make ToF-SIMS a good candidate for analyzing organic and biological samples. The main contrast between ToF-SIMS and MS-SIMS lies in the different ways of identifying the mass-to-charge ratios. Another variation is the selection of an ion beam for data analysis. In MS-SIMS, Cs^+ ions are often utilized as a primary beam, which has high ionization efficiency and enhances the sensitivity of detecting elements. It is highly effective for detecting trace and atmospheric elements, whereas ToF-SIMS usually operates Bi^+ ions and provides superior depth resolution. It is more suitable for analyzing organic and complex molecules [32].

2.2.3.3 Quadrupole Mass Analyzers

QMA consists of four parallel rods arranged in a square pattern and is commonly used in various fields. Quadrupole instruments selectively transmit ions by combining radio frequency (RF) and direct current (DC) electric fields. The ability of QMA to precisely separate ions based on their mass-to-charge ratio makes them an essential tool in many analytical applications, mainly for shallow-depth profiling. The mass resolution (300 amu) and its low transmission have limitations depending on the generation of RF voltage and the size of the rods.

2.2.4 Detectors

SIMS typically use a variety of detectors to measure the intensity of secondary ion signals, including Faraday cups (FC), electron multipliers (EM), ion image plates, and the resistive anode encoder (RAE) image detectors [5]. In general, FC can be applied to detect signals in higher ranges starting from 5×10^4 ion counts per second (c/s) and higher. EM as a sensitive detector can be utilized in lower ranges from less than 1 to around $1\times\ 10^6$ ion counts per second (c/s).

An ion image plate comprises a network of tiny electron multipliers, usually made from lead glass. The front surface of the plate is kept at ground potential, whereas the back surface is typically set to a voltage between 1 and 2 keV. The RAE image detector uses a micro-channel plate to convert ions into electrons. It records images digitally. The maximum count rates of this detector must be kept below $4\times\ 10^4$ (c/s) as it has a high but stable background count rate [32].

2.3 Quantitative Analysis

2.3.1 Sputtering Process

Upon impact of an energetic ion beam on the surface, the kinetic energy and momentum are transferred to the atoms or molecules. If the radiation energy exceeds the binding energy of atoms in a lattice, recoil atoms are created. Some primary ions may be back-scattered, secondary electrons can be ejected, photons may be produced, and some ions penetrate the sample and share part of their energy with the target atoms through electronic excitation and cascade collisions on the surface [35]. This interaction between the ion beam and the atoms on the surface is the basis of the SIMS method and is called sputtering.

The uppermost layer of the sample undergoes destruction during the measurement

process [36]. However, a significant portion of the primary ions can sputter neutral atoms and molecules, together with electrons and secondary ions at low energy. Employing different primary beams can increase the detection limit by enhancing the ionization yield. For example, using O^- and O_2^+ as a primary beam increases the detection of electropositive elements like aluminum, while Cs^+ is more effective for electronegative elements like fluorine [37].

The study of sputtering phenomena dates back to the observations made by Grove in 1853 [38] and Faraday in 1854, initially noticing metallic deposits on the glass walls of discharge tubes. Nevertheless, in the early 20th century, Goldstein revealed the evidence of the sputtering effect by performing the first ion-beam sputtering experiment, hitting the cathode with positive ions and demonstrating the disappearance of a gold coating on the glass wall facing the beam [39]. In parallel, significant experimental studies were conducted by Penning and Moubis [40], who used an axial magnetic field to aid in returning secondary electrons and reduce operating pressure. They measured sputtered material by weighing mica disks placed opposite the cathode. Guntherschulze and Meyer also contributed by employing glow discharges between heated filaments and cathodes with holes, pioneering methods to measure sputtering rates. Guntherschulze's observations eliminated back diffusion effects using cylindrical cathodes and wire anodes, deriving sputtering rates from changes in anode weight [41, 42].

Theoretical developments, such as von Hippel's evaporation theory [43], suggested that ions create localized "hot spots" on cathode surfaces, causing vaporization of surface atoms, with sputtering rates peaking at specific ion energies. Although, it did not explicitly frame the context of sputtering with these hot spots. Kingdon and Langmuir's momentum interchange theory proposed that sputtering involves atom ejection from surface crevices formed by ion impacts [44]. Later, Seeliger and Sommermeyer supported this theoretical framework by confirming the Knudsen cosine law for angular distribution of sputtered particles [45].

Stark [46] furthered the sputtering theory by proposing the hot-spot model and later a collision theory pointing to sputtering as a sequence of binary collision events. Stark's analysis incorporated conservation laws and collision cross-sections, explaining energy-dependent sputtering yields. Stark distinguishes it from von Hippel's earlier discussion of hot spots in a more general context of surface evaporation by ions. Wehner addressed the collision theory by developing an empirical formula including the sound velocity of metal, energy transfer, and sublimation heat using mercury ions to determine the sputtering thresholds for various metals [47]. Highlighted the complexities beyond local evaporation theories, contributing significantly to understanding sputtering mechanisms. Theoretical debates continued, with Lamar and Compton [48] emphasizing binary col-

lision processes in light-ion sputtering versus local evaporation in heavy-ion scenarios. These developments culminated in Timoshenko and Keywell's experiments [49], which illustrated energy-dependent sputtering ratios and proposed models akin to neutron cooling in lattices, leading to a logarithmic relationship between sputtering ratio and ion energy [50].

2.3.2 Sputtering Yield

The sputtering yield (Y) denotes the average number of atoms (including all ejected particles) sputtered from a material per incident ion under specific experimental conditions [35]. Sigmund found the sputtering yield ranges from 10^{-5} to 10^{3} atoms per incident particle [50]. The sputtering yield is given by:

$$Y = \frac{n_a}{n_i} \tag{2.5}$$

in which:

- n_a is the number of atoms sputtered from the bombarded area,
- n_i is the number of incident ions.

The sputtering ion yield is the average number of ejected ions (only includes ejected ions detected) from a material per incident ion.

$$Y_m = \frac{n_m}{n_i} \tag{2.6}$$

Here:

- n_m is the number of ions ejected from the sputtered area,

The degree of ionization yield depends on various factors, including the mass, energy, and angle of the primary ions, as well as the characteristics of the target material, such as the mass of the target atoms, the element composition of the sample, and the crystal orientation [35,51]. The relationship between ionization yields and secondary ion current depends on various parameters [52]:

$$I_m^{\pm} = \frac{I_p}{e} \cdot Y_m \cdot \eta \cdot P^{\pm} \cdot c \tag{2.7}$$

where:

- $I_m^{\pm}$ is the intensity of the secondary ion of the mass m,

- I_p is the primary ion beam current,
- Y_m is the sputtering ion yield of the target material,
- η is the ion transmission efficiency of the mass spectrometer,
- $P^{\pm}$ is the ionization probability of m,
- c is the concentration of element m.

To improve detection sensitivities, the bombardment of the sample surface with O^- and $O_2{}^+$ is a standard method to enhance the positive secondary ions yields. Conversely, to increase the negative secondary ions yields, the Cs^+ primary beam is desirable [53]. The studies indicate that the incident angle, typically around 60-80 degrees, and the use of heavier ions, compared to lighter ones, influence the enhancement of the ionization yields [35].

As reported by Werner [7], two processes contribute to the sputtering of secondary ions: physical and chemical processes [7, 50]. The physical process involves hitting the atoms on the surface with a high-energy beam, transferring the energy to the atom or molecules, knocking them out from the surface, or causing them to collide with other atoms, and electronic excitation sputtering occurs in metallic and insulator surfaces, respectively [50]. This process results in a collision cascade. Ionization of particles in this process can happen when they gain sufficient energy to break the binding forces holding them to the material's surface. This can happen through charge interaction, tunneling, auto-ionization, or Auger electron emission [7, 50].

The collision cascade model (see Figure 2.6, adopt. from [54]) stands out as the most accurate framework for elucidating the interaction between a stream of atoms and the atoms within a sample. Based on this model, the primary ion dissipates its energy through a sequence of secondary collisions with the atoms of the material. Following the generation of recoil atoms in the sample due to the collision cascade, these atoms engage with other atoms in the material. Given the random direction of recoils, some ejected atoms exit the sample surface, removing a layer approximately 1 nm thick from the sample. This layer thickness primarily hinges on the energy, angle of incidence, and beam current density of the primary ion. The remaining ejected atoms are propelled into the material to a depth of roughly 10 nm, dictated by the energy of the primary ions. The sputter ratio or sputter efficiency serves as the fundamental parameter characterizing the ion sputtering process. Chemical sputtering is when the secondary ions are sputtered from the surface directly by breaking of chemical bonds [7, 50]. Additionally, oxidation plays a crucial role in this type of sputtering [55]. Theories for the inelastic processes suggest either electronic excitations due to atomic collisions or electron tunneling [56, 57]. These two approaches

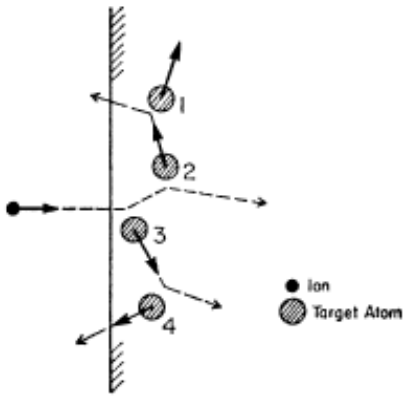

Figure 2.6: Series of collision processes leading to sputtering of atoms 2 and 4 (Taken from [54]).

differ conceptually. The electron-tunneling model describes the interaction between the discrete electronic levels of the sputtered atom and the continuous electronic states of the solid, with the Fermi level playing a crucial role as it separates occupied and unoccupied states. In contrast, collision models do not explicitly involve the Fermi level [58].

2.4 Matrix Effects

The influence of oxygen and cesium on sputtered ion yields exemplifies the broader phenomenon where ion yields are significantly affected by changes in the surface composition from which ions are ejected. This effect occurs when the sample matrix influences the ionization yields. This influence is called the matrix effect, which is typically unpredictable and poorly understood. This resulted in a considerable challenge to the analytical power of the SIMS technique [9, 29, 59–61]. The presence of different elements in the matrix can influence the ionization efficiency of analyte species, potentially resulting in inaccurate quantification (see Figure 2.7, adopt. from [62]). Therefore, developing a method that considers the matrix effect and enhances the accuracy of the measurement is necessary. According to Datz [61], matrix effects can be categorized into three different types: alloy effects, compound effects, and sputtering effects. Alloy effects arise when the surface's composition alters, but its physical properties do not change, and the surface remains metallic. Compound effects come from transforming a metallic conductor into an insulator, such as in oxides, halides, and other ionic compounds. Initially, cesium's effects might seem to fall under the alloy category. Still, it has been demonstrated that cesium forms charge-transfer insulators with many metals that are ionic and have band-gap properties [63, 64]. Consequently, the mechanism by which cesium enhances negative

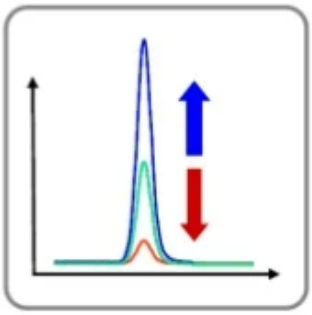

Figure 2.7: Schematic representation of matrix effects on SIMS signal, illustrating signal enhancement (dark blue line) or suppression (orange line) (Taken from [62]).

ion yields likely mirrors the mechanism by which oxygen enhances positive ion yields. Sputtering effects are compound effects and arise from changes in the quantity of oxygen or cesium on the sputtered surface [29, 61].

Scientists have developed theories to explain ion ejection during sputtering, but understanding remains limited, especially for complex surfaces. The simplest theories envision atoms being ejected from a surface, remaining unchanged, and having the same structure. On a clean metal surface, an electronegative atom tends to attract electrons, becoming a negative ion by gaining an extra electron. As this atom moves away from the metal surface, it loses the extra electron and returns to a neutral state. The potential energy levels for the ionized (negative ion) and neutral states intersect at a distance from the surface. In a one-electron model, this intersection occurs where the atom's energy level matches the Fermi level of the metal, allowing resonant electron transfer back to the metal. The Landau-Zener-Stuekelburg model describes how the probability of an atom remaining ionized decreases exponentially with the distance at which energy levels cross, influenced by the atom's velocity at that point. This explains why different isotopes of the same element have different ionization efficiencies, assuming they have the same energy when ejected [29, 61].

The crossing distance depends on two factors: the surface's work function and the electron affinity of the sputtered atom. If the electron affinity of an atom is higher, its energy level is lower. Changes in the work function affect how different materials behave during sputtering, and changes in electron affinity explain why different elements have different sensitivities. For compounds or insulators, the situation is more complex. Insulators have low electron density at the Fermi level, so electron transfer there is less important. Instead, electron transfer between the atom and the bands (energy levels) of the insulator's surface is more significant if the surface structure remains unchanged. This means that for insulators, the important electron transfers happen between the atom and

the energy levels of the insulator's surface rather than the Fermi level [9, 29].

During sputtering, the surface becomes disordered, and in such chaotic conditions, the usual concepts of how electrons move through a material (bulk band structure theory) might not apply. Each ejected atom leaves a defect on the surface, influencing subsequent ionization processes. This understanding forms the basis for comprehending matrix effects in SIMS analysis. When a negatively charged atom (anion) leaves its spot, taking an electron with it, a vacancy forms where the anion used to be, causing an energy drop in the conduction band. This vacancy stabilizes as the anion moves away. The likelihood that the ion survives after ejection depends on where the energy levels of this vacancy and the atom's level meet. This process is similar to what occurs in metals.

The distance where energy levels cross is influenced by the electron affinity or ionization potential of the atom being ejected and the band structure of the surface. A larger band gap indicates higher energy levels in the valence band, resulting in a greater distance where these energy levels intersect. When a narrow band gap metal with a low electropositivity is sputtered from its oxide, the ability to form ions will be lower than when it is sputtered from the oxide of a highly electropositive metal with a wider band gap. The stronger the polarity of the bonding (indicated by a larger band gap), the greater the production of ions. Conversely, a metal with higher electropositivity produces fewer secondary ions when sputtered from the oxide of a metal with lower electropositivity [9, 29, 61].

Using oxygen or cesium primary ions in sputtering reveals matrix effects inversely correlated with the amount of sputtered material or sputtering yield. Since ionization efficiencies often change with the second or third power of the oxygen or cesium concentration on the surface, even minor variations in sputtering yield can cause significant fluctuations in ionization efficiency. Deline et al. [59] proposed a unified explanation for secondary ion yields, discovering that the chemical composition did not affect ionization efficiency [9]. Witmaack critically scrutinized his proposition [60]. However, subsequent research indicated that the change in the material composition strongly impacts ion yields, meaning the composition of the surface plays a crucial role in matrix effects. Williams' review of ion emission models, including the "bond-breaking," work function, band structure, molecular, and surface-polarization models, highlights the complexity in predicting secondary ion yields accurately [29, 61, 65].

Nevertheless, none of these theoretical frameworks garner sufficient support from experimental evidence to predict secondary ion yields with the desired accuracy. To date, no systematic investigations have delved into the ionization probability of ternary compound semiconductors under continuous bombardment by a Cs^+ primary ion beam. Current research aims to investigate the influence of the matrix effect in ternary semiconductor compounds PbSnTe and CdZnO under specific conditions and its relation with the

electronic properties of the material.

2.5 Theory of Study

The ability of the SIMS method for accurate quantitative measurements is limited due to an insufficient understanding of the formation of secondary ions. To overcome this issue, a key factor is the ionization probability, which is the possibility of a sputtered particle becoming a charged ion, either positively or negatively. It is essential to know how the ionization probability is influenced by physical characteristics like work function (the minimum energy required to release an electron from a surface), the electron affinity (the amount of energy released after capturing an electron by an atom) and ionization potential of atom [66–68].

Multiple methods have been utilized to measure the work function of a solid, including techniques such as the Kelvin probe, photo emission, secondary electrons, and secondary ions [69–75]. The method using secondary ions focuses on identifying the initial point of their energy distribution. The observable shift in energy distribution, reflecting changes in potential between the sample and the energy analyzer, provides an effective way to monitor variations in the work function in real time. Findings indicated reduced work function value by adsorbing alkali metals on the surface [69, 76]. Gnaser has explored how adding cesium to surfaces affects either positive or negative ion emissions, revealing insights into the relationship between ion emission and ionization probability due to the variation in work function.

Efforts to estimate the work function using secondary ion analysis have been undertaken by researchers like Blaise and Slodzian [77], who studied the energy distribution of sputtered ions. Similarly, Yamazaki et al. [71] investigated how the work function influences ionization efficiency in SIMS by examining boron implantation into silicon. In metal [78], the electron in the valence band is characterized by their Fermi level, which represents the border of the occupied energy levels and empty ones, ϕ is equal to its electron affinity of material (A_m) [69]. Eq. 2.8 displays the estimation of ϕ in metals. E_{vac} represents the energy in the vacuum level and E_F the energy at the Fermi level.

$$\phi = E_{vac} - E_F \tag{2.8}$$

In semiconductors, the electron affinity plays a crucial role alongside the work function. It denotes the energy difference between the lowest point of the conduction band and the vacuum level [79]. Within n-type semiconductors, the Fermi level aligns near the conduction band edge, and the work function closely follows the electron affinity. In

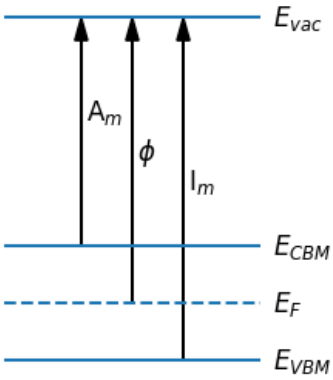

Figure 2.8: Schematic representation of band gap for semi-insulator semiconductor.

p-type semiconductors, the Fermi level resides near the valence band edge, and the work function consistently exceeds the electron affinity [55, 71]. Due to the band gap, ϕ is greater or equal to A_m in semiconductors. As schematically depicted in Figure 2.8, the A_m represents the energy difference between the vacuum level and the conduction band. Its relationship with ionization potential (I) can be expressed using Eqs. 2.9 and 2.10 [69].

$$A_m = E_{vac} - E_c \tag{2.9}$$

$$I = E_{vac} - E_v \tag{2.10}$$

E_c and E_v display the energy on the conduction and valence bands. By substituting Eq. 2.10 into Eq. 2.8, the work function of semiconductors is express by Eq. 2.11:

$$\phi = I - (E_F - E_v) \tag{2.11}$$

Yu [55, 58, 68, 80–82] conducted an extensive study to explain the correlation between the ionization probability of sputtered ions and the physical properties of ejected particles in case of the metallic surface. He discussed two main factors: ionization potential and electron affinity, which correspond to positive and negative ionization [55, 67, 71, 83, 84], respectively. The relation is expressed as follows:

$$P^- \sim e^{A_e - \phi} \tag{2.12}$$

$$P^{+} \sim e^{\phi - I_e} \tag{2.13}$$

The negative secondary ion yield enhancement has been reported to exhibit an exponential relationship with the electron affinities of the sputtered atoms (A_e), Eq. 2.12. The positive secondary ion yield is exponentially related to the ionization potential of sputtered atoms (I_e), Eq. 2.13 [55, 71]. A reduction in a work function makes it easier for electrons to be released from the surface. More and more electrons above the surface are easily captured by Cs^{+} ions [80].

In the case of semiconductors, the ionization probability of secondary ions emitted during sputtering is dependent exponentially on the work function, and the electron affinity of the material (A_m), as depicted in Eqs. 2.14 and 2.15.

$$P^{-} \sim e^{A_e - \phi} \tag{2.14}$$

$$P^{+} \sim e^{A_m - I_e} \tag{2.15}$$

Changes in chemical composition typically influence the band gap energy, thereby concurrently impacting ϕ and A_m. Unlike materials that display band gap bowing, this relationship is generally linear [55]. In this study, the electronic properties of PbSnTe were characterized based on the appropriate application of the above theory to the SIMS method, creating a data analysis method that is completely new in the context of ternary semiconductor characterization.

2.6 Quantification of SIMS Data

2.6.1 Depth Profile

In SIMS, depth profiling involves bombarding the sample surface with ions to progressively sputter layers, enabling the analysis of elemental distribution and composition throughout the sample's depth. As sputtering proceeds, species are continuously monitored, and their profiles are tracked as the analysis penetrates subsequent layers. SIMS provides detailed information about the sample's structure by measuring the secondary ions ejected at each layer. Maintaining a constant primary current is crucial, as the depth of the crater formed during depth profiling depends on both the primary beam intensity and the sputtering duration [85]. The analysis during a depth profile is conducted at the center of a crater to avoid the influence of edge effect [86].

In depth profiling, converting the depth scale after measurement requires knowledge of the sample thickness. If the thickness is unknown, the sputter rate (SR) can be used, which is defined as the ratio of the crater's depth (d) nm to the sputtering time (t) s, as expressed in Eq. 2.16:

$$\mathrm{SR} = \frac{\mathrm{d}}{\mathrm{t}} \tag{2.16}$$

This relationship provides a practical method for calibrating depth profiles when sample thickness is not directly measurable [87].

2.6.2 Concentration Profile

The Relative Sensitivity Factor (RSF) method is the predominant quantification technique in SIMS. The approach relies on determining a scaling factor through SIMS measurements of a known elemental standard. RSF denotes the instrument's sensitivity to detect various elements or isotopes within a sample. It is calculated as the ratio of the ion signal for a specific element or isotope to that for a reference element or isotope. Various factors, such as primary ion species and energy, matrix composition, and ionization efficiency of the elements, influence its value.

RSF Correction is employed to address matrix effects in SIMS analysis. This correction involves adjusting the measured intensities of analyte species based on their RSF values, compensating for variations in ionization efficiency induced by matrix effects. RSF Correction significantly enhances the accuracy and precision of SIMS measurements, particularly in quantitative analysis. RSF values are typically determined from the standards, which are the ion-implanted materials, where the RSF of species is quantified using the given formula:

$$\mathrm{RSF} = \frac{\phi \cdot a \cdot I_{\mathrm{r}} \cdot t}{d \cdot I_{\mathrm{e}} - d \cdot I_{\mathrm{b}} \cdot a} \times \frac{EM}{FC} \tag{2.17}$$

where,

- ϕ is the dose (in atoms/cm^2) from a known standard.
- a denotes the number of analysis iterations.
- $\frac{EM}{FC}$ represents the ratio of electron multiplier to Faraday cup efficiency.
- d is the depth of the crater.
- I_{e} is the total intensity of the analyzed elements or implanted species.
- I_{b} is the intensity of the background ions.
- t is the duration of the measurement.

The concentration profile of a specific element varies with the depth of the material. Typically, this profile is depicted as a smooth curve of concentration (C) plotted versus depth (x) in the sample, often using a logarithmic scale. By determination of RSF from a measurement of SIMS standard, the concentration of elements can be calculated from the raw SIMS data of a studied sample using the following formula:

$$\mathrm{C} = \mathrm{RSF} \times \frac{\mathrm{I_e}}{\mathrm{I_r}} \tag{2.18}$$

here,

- C is the atom density (atoms/cm^3) in the material.
- I_e and I_r represent the secondary ion intensity (counts/s) of the analyzed element and the reference matrix element, respectively.

2.6.3 Mass Spectra

A mass spectrum is obtained by bombarding the sample surface and scanning the mass range with the mass spectrometer. This spectrum is a graphical representation of signal intensity versus the m/z. Each peak signifies ions produced from the sputtering surface, with its position denoting its m/z value. The intensity or height of each peak reflects the ion's abundance.

2.6.4 Energy Distribution Profile

When the primary beam hits the sample's surface, it generates random collisions that can eject secondary ions with varying energy ranges. This means secondary ions formed from different local environments (neighborhoods) differ in terms of atomic bonding and the surrounding chemical environment, resulting in different energy distribution profiles for each element. The energy distribution of secondary ions usually peaks at low energies (a few eV). Still, the distribution may be narrow or broad, with peaks extending to higher energies (over 100 eV), depending on the type of ion. The secondary ions with a specific range of velocity (the kinetic energy) can go through a particular slit and then to the mass analyzer. Therefore, if the velocity of secondary ions is lower or higher than the adjusted potential, they may not go through the energy gate or may be deflected from the detector.

In a typical SIMS experiment, an energy scan is performed by varying the voltage applied to the sample, usually within a range of about -150 to 150 volts (V). A typical setting of the device potential applied to the sample starts from 4.5 kV and -4.5 kV for positive and negative secondary ions. A voltage offset technique is employed to enhance

the detection of mono-atomic ions over multi-atomic ones, as mono-atomic ions often exhibit broader energy distributions. When the accelerating voltage is reduced (offset), mono-atomic ions generally retain sufficient energy to pass through the energy slits. In contrast, multi-atomic ions are less likely to be detected [32].

The potential applied to the sample affects the overall impact energy of primary ions based on whether positive or negative secondary ions are detected. For example, in the case of positive secondary ions, the total energy of the primary beam impacting the surface would be the difference between the initial energy (10 keV) and the sample bias (4.5 keV), resulting in a total impact energy of 5.5 keV. Finally, adjusting the initial sample potential can achieve an energy distribution profile.

2.6.5 Ion Images

SIMS can utilize focused ion beams to generate images from the secondary ions sputtered from the sample's surface. This technique is similar to SEM, which employs an electron beam to irradiate the surface and collect secondary electrons to produce the image.

2.7 Instruments Used in This Work

This study employed a CAMECA IMS6F magnetic sector SIMS (Figure 2.9), which operates within a high vacuum environment during measurements. Our instrument allows for selecting Cs and O as primary beam options, with energy ranging from 0.5 to 20 keV [5, 35]. In our device, the potential that accelerates the secondary ions into a mass spectrometer is about 4.5 to 10 keV. IMS-6F has two detectors: an electron multiplier and a Faraday cup. The electron multiplier is much more sensitive and can be used for intensities ranging from about 1 to approximately 10^6 counts per second. A Faraday cup for measuring higher intensity signals [88]. A ToF-SIMS V spectrometer manufactured by IONTOF GmbH was used to acquire the data for time-of-flight secondary ion mass spectrometry (Figure 2.10).

Moreover, the depth of a crater created during the sample's bombardment with a primary beam is determined using the DEKTAK 6M stylus profilometer. A Hitachi SU-70 scanning electron microscope (SEM) with a Thermo Scientific energy-dispersive X-ray (EDX) spectrometer was applied to estimate the content in $Cd_{1-x}Zn_xO$ thin films. A reflection high-energy electron diffraction (RHEED) was utilized to analyze the growth mode of the $Pb_{1-x}Sn_xTe$. Their elemental composition was investigated using a FlexSEM 1000 SEM (Hitachi) equipped with an EDX spectrometer (Oxford Instruments).

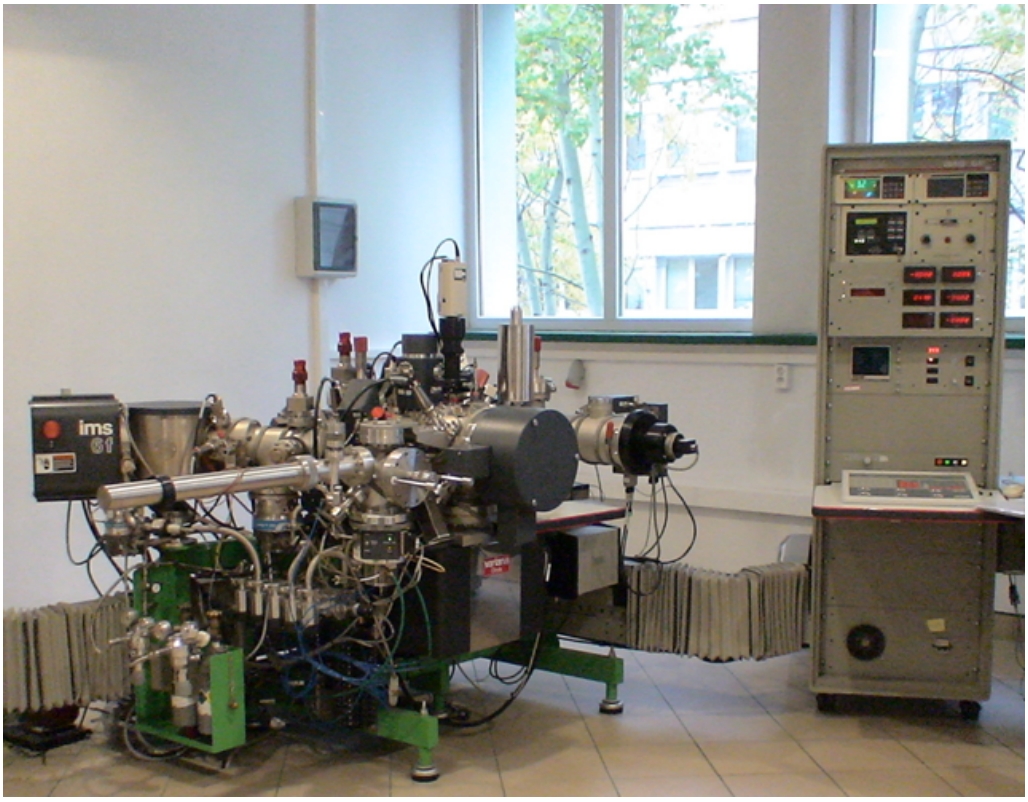

Figure 2.9: Cameca IM6F magnetic sector SIMS used in this study.

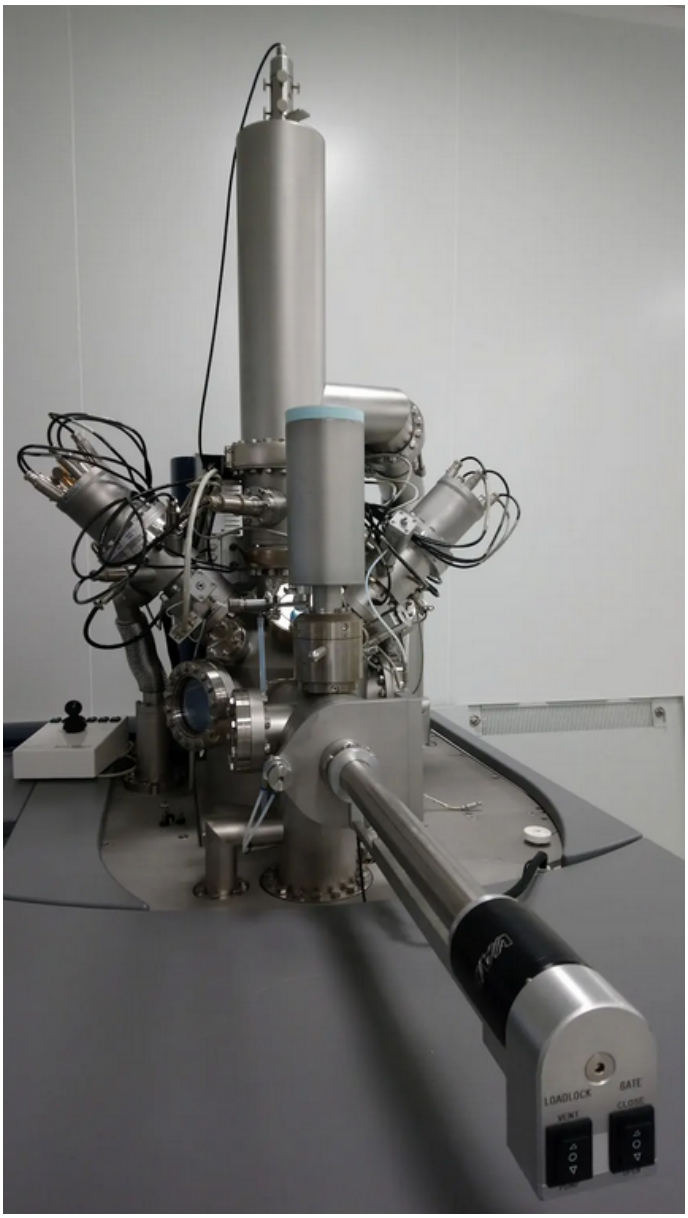

Figure 2.10: A ToF-SIMS V spectrometer, IONTOF GmbH SIMS used in this study.

Chapter 3

Materials and Measurements

3.1 Introduction

Ternary compound semiconductors represent a significant class of materials in semiconductor research due to their versatile electronic and optical properties. These materials are formed by incorporating a third element into a binary compound semiconductor, which allows for fine-tuning of the material's properties to meet specific application requirements. The ability to adjust the composition in ternary compounds leads to tunable band gaps, which is particularly advantageous for designing optoelectronic devices like light-emitting diodes (LEDs), laser diodes, and photodetectors. Precise control over their structural and electronic characteristics makes ternary compound semiconductors a cornerstone in advancing modern electronic and photonic technologies [89, 90]. This chapter investigates two essential ternary compounds: $Cd_{1-x}Zn_xO$ and $Pb_{1-x}Sn_xTe$. These compounds are important in semiconductor physics and spectroscopic analysis, driving our study forward. Our keen interest in scrutinizing these materials and exploring cutting-edge topics stems from our endeavor to understand the influence of the matrix effects on ion yield in the SIMS method due to the change in material composition.

3.2 Ternary Compound Semiconductors

The foundation of the electronics industry lies in semiconductor devices. The semiconductor industry began in 1947 when Bell Labs introduced the first semiconductor transistor. Following this breakthrough, semiconductor technology rapidly advanced, particularly during the 1970s, when III-V compound semiconductors, especially gallium arsenide (GaAs)-based lasers, garnered significant attention. The introduction of silicon (Si) revolutionized the industry due to its applications in data storage and computing circuits. However, Si's indirect band gap renders it unsuitable for optoelectronic devices. GaAs, with its direct band gap, emerged as a solution. Nonetheless, the increasing demand for ultraviolet (UV) light-emitting devices shifted the focus towards wide-bandgap semiconductors such as SiC, GaN, and ZnO [91].

The initial understanding of the electronic energy band structures in narrow-gap semiconductors originated from a theoretical model proposed by Kane in 1957, which was primarily based on the semiconductor InSb [92]. Following Kane's model, researchers

extended their investigations to other narrow-bandgap semiconductor materials such as PbTe, PbSnTe, HgCdTe, and various III-V compounds (e.g., InAs, InSb, GaSb) [93] gained attention due to their similar electronic properties and potential applications in infrared detectors, thermoelectric devices, and optoelectronic systems. The advancement in narrow-bandgap semiconductor physics is intricately linked to infrared detection technology [92].

The crystal structure of semiconductors often lacks perfect order. This lack of order leads to a random distribution of lattice atoms, disrupting the periodic lattice potential and causing variations in bond length, which induce local strain. As a result, Vegard's law does not apply to specific physical parameters such as bandgap energy (Eg), effective mass (m^*), and mobility (μ) in these compounds. Vegard's Law is often used to estimate the composition of semiconductor alloys based on X-ray diffraction or other experimental measurements of lattice parameters. For a ternary semiconductor $A_xB_{1-x}C$, an alloy of two binary semiconductors (AC and BC), the physical property parameter can be expressed as:

$$T_{ij}(x) = (1-x)B_i + xB_j + x(1-x)C_{ij} \tag{3.1}$$

Here, Tij(x) represents the physical property of the ternary alloy composed of binaries i and j, Bi, and Bj are the properties of the binary semiconductors, and C_{ij} is the ternary bowing parameter that accounts for deviations from linear interpolation between the binaries. Consequently, $E_g = a + bx + Cx^2$ gives the bandgap energy and composition relationship, where C is the bowing parameter, typically ranging from 0.2 to 0.8 in III-V compounds. Additionally, in ternary alloys, when mixing a direct bandgap binary with an indirect bandgap binary, the lowest conduction band can shift from direct to indirect at a specific composition, limiting the material's efficiency as a light emitter [19].

3.3 Cadmium Zinc Oxide

3.3.1 General Overview

II-VI semiconductors have gained considerable attention for their potential applications across various fields for years. These semiconductors consist of group IIB metallic elements like Cd, Zn, and Hg, paired with group VI nonmetallic elements such as O, S, Se, and Te. Among these elements, zinc oxide (ZnO) stands out due to its exceptional properties, making it indispensable in applications ranging from varistors to sensors and optoelectronic devices. Cadmium oxide (CdO) is another significant II-VI semiconductor, noted for its outstanding optoelectronic characteristics [10–12].

The ternary compound $Zn_xCd_{1-x}O$ is anticipated to cover a broad spectral range from ultraviolet to yellow wavelengths due to its adjustable bandgap [94]. While significant research has been conducted on the structural, optical, and electrical properties of $Zn_xCd_{1-x}O$, there is limited work on the quantification and precise calibration of these materials using secondary ion mass spectrometry.

This study explores CdZnO, a ternary compound semiconductor that exhibits intriguing properties, such as tunable bandgap – by varying the ratio of Cd to Zn. Increasing Zn content widens the bandgap while increasing Cd content narrows it, affecting its optoelectronic characteristics. Although CdZnO has been extensively studied for its structural and optical properties, no prior investigations have employed SIMS to analyze its material composition. This study aims to fill that gap by using SIMS to examine the matrix effects and accurately determine the elemental distribution in CdZnO thin films.

By employing SIMS, we aim to establish a precise calibration for analyzing CdZnO, which is crucial for understanding how its composition influences electronic properties. Given the absence of SIMS-specific calibration curves for this material, our work is novel and will contribute significantly to the field of semiconductor analysis. Our findings will also provide insights into the broader applicability of SIMS for similar ternary semiconductors, especially in cases where matrix effects pose challenges for composition determination.

3.3.2 Background

The binary compounds ZnO and CdO possess different crystalline structures: ZnO adopts a wurtzite structure (Zn cations tetrahedrally coordinated by O ions) [95,96] with a direct bandgap of approximately 3.37 eV [97,98]. In comparison, CdO adopts a rock salt structure (Cd cations octahedrally coordinated by O ions) with a bandgap ranging from 2.2 eV [99]

to 2.4 eV [100] at room temperature. The initial study on this ternary compound by Choi et al. [101] demonstrated that decreasing the Zn content (x value) reduces the electrical resistivity, optical transmittance, and bandgap of $Zn_xCd_{1-x}O$. Subsequent research has explored various properties of this compound both experimentally [94, 102–107] and theoretically [108, 109].

Recent studies on the crystalline structure of $Zn_xCd_{1-x}O$ nanopowder report a transition from rocksalt CdO to wurtzite ZnO as the Zn composition increases [110]. Increasing the Cd content decreases the optical bandgap [107]. While significant research has been conducted on the structural, optical, and electrical properties of $Zn_xCd_{1-x}O$, there is limited work on the quantification and precise calibration of these materials using secondary ion mass spectrometry. Most existing studies focus on the impact of annealing on the properties of CdZnO.

This research aims to bridge this gap by estimating the calibration curve for CdZnO using SIMS. To do this, establishing a relationship between the secondary ions' intensity and the concentration of matrix elements in $Cd_{1-x}Zn_xO$ is required. The accurate calibration curves can be constructed by analyzing uniform samples with known contents. This approach not only gives a better understanding of the properties of CdZnO but also can improve the estimation of content in ternary compounds when the matrix effects can affect the measurement.

3.3.3 Applications

The band gap of ZnO can be altered by introducing Cd [111, 112] which makes CdZnO a good candidate in a wide range of applications such as optoelectronic devices [10, 113], photodetectors [114, 115], various sensors [116, 117], and fuel cells and photocatalysis [11, 118], high-temperature electronics, light detectors, laser sources, oxide-based quantum devices [12].

3.3.4 Growth Process of $Cd_{1-x}Zn_xO$ Thin Films

$Cd_{1-x}Zn_xO$ thin films were grown on c-plane (00.1) sapphire substrates using MBE with a Compact 21 Riber system. This MBE setup uses a radio-frequency (RF) oxygen plasma source and double-zone Knudsen effusion cells that provide the elemental O, Cd, and Zn sources. Cadmium (Cd) with 6 N purity, sourced from JX Nippon Mining and Metal Corporation, and zinc (Zn) with 6 N purity were used, while oxygen plasma was generated by the RF cell.

Prior to film growth, the Al_2O_3 substrates were cleaned chemically in a 1:1 mixture of H_2SO_4 and H_2O_2. The substrates underwent degassing at 150°C in the load chamber

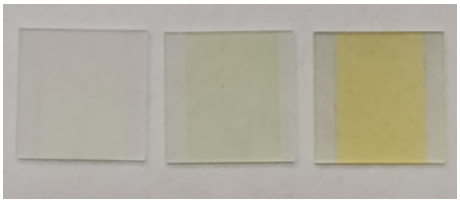

Figure 3.1: An example of $Cd_{1-x}Zn_xO$ thin films used in the first series. The color of the samples depends on the Cd content.

for 1 hour and were then annealed at 700°C in the growth chamber. The growth of the $Cd_{1-x}Zn_xO$ films was conducted with a constant oxygen flow rate of 3 sccm, with the oxygen plasma activated at approximately 240 W. The films were deposited at a temperature of 360°C, as measured by a thermocouple, over 1 hour. The Cd (x) composition within the $Cd_{1-x}Zn_xO$ films was varied by adjusting the fluxes of Cd and Zn through the respective effusion cells.

This study focuses on two distinct series of $Cd_{1-x}Zn_xO$ samples: The first series includes chemically homogeneous samples with progressively increasing Cd content, ranging from 0 to 0.6, as specified in Table 3.1. Each sample in this series has a unique and fixed Cd composition, which establishes a calibration curve for analyzing the SIMS signal ratio (see Figure 3.1). The second series comprises thin samples for which accurate Cd content determination by EDX is challenging.

The objective is to estimate the Cd content using the RSF and calibration curve data and compare the results. The compositional analysis of Cd and Zn in the $Cd_{1-x}Zn_xO$ thin films was performed using an EDX spectrometer with a silicon drift X-ray detector and Noran System 7, set at an accelerating voltage of 8 kV.

Table 3.1: The content of $Cd_{1-x}Zn_xO$ samples.

Sample	x_{Cd}
1	0.0000
2	0.0001
3	0.0010
4	0.0020
5	0.0080
6	0.0180
7	0.1900
8	0.2800
9	0.3900
10	0.6000

3.3.5 Measurement Conditions

For MS-SIMS, a Cs^+ primary beam energy of 5.5 keV at a current of 50 nA was applied to analyze the material. The beam was rastered over the area of $250\mu\text{m} \times 250\mu\text{m}$, and secondary ions were collected from a region of $60\mu\text{m}$ in diameter. In the case of ToF-SIMS, Bi^+ primary beam with an energy of 30 keV at a current of 1.1 pA was conducted over an area of $50\mu\text{m} \times 50\mu\text{m}$ as the analysis beam. A Cs^+ ion beam over an area of $200\mu\text{m} \times 200\mu\text{m}$ was performed to sputter the material for in-depth analysis. The following species were measured using both instruments: $^{114}Cd^+$, $^{64}Zn^+$, $^{114}CdCs^+$, $^{64}ZnCs^+$. Due to the zero electron affinity of Zn, it can not be detected as a negative ion in our experiment, so we just utilized positive secondary ions [119].

3.4 Lead Tin Telluride

3.4.1 General Overview

$Pb_{1-x}Sn_xTe$ is a ternary compound semiconductor with notable properties, including its classification as a topological insulator, a material insulating in bulk but conducting electricity on the surface. No investigations have been shown to determine the exact composition of this compound for studying material-based superlattices or heterostructures.

This study fills that gap by using SIMS to examine the matrix effects and accurately determine the elemental distribution in $Pb_{1-x}Sn_xTe$ thin films. By employing SIMS, we aim to establish a precise method for analyzing the content of $Pb_{1-x}Sn_xTe$ which is crucial for understanding how its composition influences its electronic properties. Given the absence of SIMS-specific calibration curves for this material, our work is novel and will contribute significantly to the field of semiconductor analysis. Our findings will also provide insights into the broader applicability of SIMS for similar ternary semiconductors, especially in cases where matrix effects pose challenges for composition determination.

3.4.2 Background

Research into the properties of lead telluride (PbTe), with a bandgap of 0.32 eV, has expanded to investigate the effects of alloying it with other elements. Tin telluride (SnTe), with a bandgap of 0.18 eV, was selected due to its structural and properties similarities with PbTe. By alloying PbTe and SnTe, researchers synthesized the ternary compound $Pb_{1-x}Sn_xTe$ which exhibited intriguing and advantageous properties compared to its binary constituents [120]. PbSnTe is a well-explored semiconductor material, extensively studied for its electronic and thermoelectric attributes, both experimentally [121–127] and theoretically [17, 128, 129].

The material has a narrow energy gap and exhibits an unusual relationship between band energies and the content of Sn. This phenomenon is elucidated by the band inversion model proposed by Dimmock et al. [120], wherein the valence and conduction bands in SnTe are inverted relative to PbTe. Consequently, the energy gap of $Pb_{1-x}Sn_xTe$ initially decreases with increasing Sn content (x) and eventually disappears at an intermediate alloy composition, where the valence and conduction bands intersect ($E_g = 0$). Further increases in Sn content (x) beyond this point lead to an additional increase in the band gap of this material. Moreover, the position of the band crossing depends on the temperature of measurement. Ocio [130] concurrently discovered that Sn content variations affect the band energy separation of the material.

Further contributing to understanding lead chalcogenides, H. Preier presented a comprehensive overview, summarizing the state-of-the-art knowledge on this material in 1979 [131]. 1999, Ferreira et al. reported direct experimental evidence of the band inversion in this ternary compound using optical transmission measurements [132]. Since 2009, $Pb_{1-x}Sn_xTe$ semiconductors have experienced a resurgence of interest. This renewed attention stems from research highlighting the unusual evolution of the band gap in $Pb_{1-x}Sn_xTe$ nanocrystals due to band inversion [133]. Unlike the massive research conducted on the structure properties of PbSnTe, still the quantification of the content of these materials is a fundamental challenge in heterostructures and superlattices. The calibration curves developed in this work aim to fill this gap, providing a valuable tool for precise compositional analysis in future studies of PbSnTe.

3.4.3 Applications

The broad application of PbSnTe made them popular across a variety of fields like optoelectronic devices: infrared detectors [13], lasers [14,15], thermoelectric converters [134], solar cell, and memory devices [16]. Also, it is applicable in quantum computing, advanced electronic [17], and spintronic devices [18].

3.4.4 Growth Process of $Pb_{1-x}Sn_xTe$ Thin Films

The ternary $Pb_{1-x}Sn_xTe$ compounds were synthesized using a home-built designed MBE system, covering the entire composition range from $x = 0$ to $x = 1$. The films were grown in an ultra-high vacuum environment, with a base pressure of 10^{-9} mbar, using SnTe and elemental Pb and Te sources. The deposition was conducted at temperatures ranging from 270°C to 310°C, with a beam equivalent pressure of 7×10^{-5} Pa, resulting in a growth rate of about 0.13 nm/s. Two different substrates were used: n-GaAs(111)B [135], and GaAs(100)B [136] for SIMS and BaF_2(100) for Hall effect measurements. The substrates were heated to approximately 600°C to remove surface oxides. The film thicknesses varied from 0.4 to 0.9 µm.

This research featured two series of $Pb_{1-x}Sn_xTe$ samples, each serving a specific purpose. The first series included chemically uniform samples with incremental variations in Sn concentration from $x = 0$ to $x = 1$. These samples were used to explore the impact of different Sn content on the band structure and to analyze SIMS signal ratios 3.2 (see Figure 3.2). The second series comprised graded samples where the Sn content changed gradually within each sample. This approach was intended to study continuous variations in the band structure properties, enabling the change in the energy distribution profile of secondary ions analyzed via SIMS. Chemical composition analysis was performed with

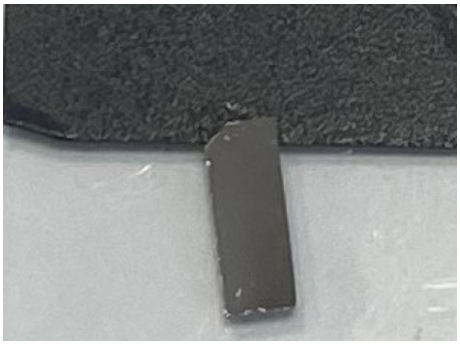

Figure 3.2: An example of $Pb_{1-x}Sn_xTe$ thin films used in the first series.

an EDX spectrometer set at an accelerating voltage of 15 kV. Hall effect measurements at room temperature were used to assess carrier concentrations.

Table 3.2: The content and thickness of $Pb_{1-x}Sn_xTe$ samples.

Sample	x_{Sn}	**d** $(\mu\mathrm{m})$
1	0.84	0.45
2	0.71	0.57
3	0.58	0.57
4	0.57	0.40
5	0.50	0.65
6	0.37	0.48
7	0.36	0.61
8	0.29	0.60
9	0.21	0.70
10	0.19	0.60
11	0.11	0.67
12	0.06	0.84

3.4.5 Measurement Conditions

The measurements were conducted using the MS-SIMS instrument. Samples were measured under high vacuum conditions with a system pressure of approximately 1.33×10^{-8} Pa. The primary ion was directed on the sample surface at an angle of about 30 degrees to the normal plane. The sputter rates for positive secondary ions were 3 and 5 (nm/s) for negative secondary ions. Primary currents for both primary beams were kept at 50 nA. Also, the raster size was about 150×150 $(\mu\mathrm{m})$, and the secondary ions were collected from a region of 60 μm in diameter. Positive ions were analyzed using $Cs^{\pm}$ primary beam at the energy of 5.5 keV and negative ions at 14.5 keV. The species measured were $^{118}Sn^{+}$, $^{208}Pb^{+}$, $^{118}SnCs^{+}$, $^{208}PbCs^{+}$, and $^{118}Sn^{-}$, $^{208}Pb^{-}$.

Due to the high electronegativity of Te (2.1 eV), a strong negative secondary ion signal of Te at a mass of 120 amu is detectable [67]. To prevent overlap between the $^{120}Te^-$ and $^{120}Sn^-$ signals at this mass, the isotope $^{118}Sn^-$ was measured instead. This setup allows for the collection of all signals using a single detector, specifically an electron multiplier.

Chapter 4

Results: Summary of Publications

4.1 Quantification of CdZnO

4.1.1 Previous Research on the Calibration Curve Method

The use of SIMS for the compositional analysis of matrix elements in ternary semiconductors has been explored in a limited number of studies. Although the calibration curve method has shown potential for accurate compositional analysis, its application to ternary systems remains underdeveloped. In this context, our study extensively investigates and refines this method for ternary semiconductors, focusing on improving its accuracy and applicability.

Gao [19] pioneered a SIMS technique employing Cs^+ primary ion bombardment and the detection of MCs^+ molecular ions for compositional analysis of AlGaAs/GaAs. This method demonstrated the ability to mitigate matrix effects, achieving linear ion yields independent of the matrix composition with an accuracy better than 2%.

Building on this, Gnaser [20] et al. applied Cs^+ primary ions and MCs^+ molecular ions for depth profiling of Zn-doped InGaAsP/InP multilayer samples. Their results showed that MCs^+ intensities closely correlate with the elemental concentrations, providing a more accurate alternative to traditional atomic ion yields. This method effectively reduced the influence of matrix effects, enabling semi-quantitative analysis of elements such as Zn and Cd, particularly at complex multilayer interfaces.

Wang [21] et al. further refined these techniques for determining Cd composition in HgCdTe. By measuring the ratio of $CdCs^+$ to $HgCs^+$ secondary ion intensities, they established a calibration curve that accurately mapped Cd composition. Their method delivered precise Cd profiles for multilayer HgCdTe samples with minimal error, especially when employing an internal reference point for calibration.

These studies highlight the evolution of SIMS techniques in mitigating matrix effects and improving quantification accuracy. The calibration curve method developed by Wang, in particular, closely aligns with the approach taken in this work but has been adapted here for CdZnO thin films. Where calibration curves are established using the ratios of $CdCs^+/ZnCs^+$ and Cd^+/Zn^+ secondary ion intensities. These intensity ratios closely correlate with the Cd composition in thin films, enabling precise quantification of Cd content. The novelty of this work lies in the use of two separate calibration curves: one derived from molecular ion intensities ($CdCs^+/ZnCs^+$) and the other from atomic ion

intensities (Cd^+/Zn^+). This dual-calibration approach provides a deeper understanding of ionization behavior in CdZnO thin films and enhances analytical accuracy. Furthermore, the method is validated using two distinct SIMS techniques—MS SIMS and TOF SIMS—allowing cross-comparison and demonstrating the robustness and versatility of the approach. Compared to the traditional RSF method, which requires multiple standards and is prone to matrix effect assumptions, the proposed method offers improved precision, reduced matrix effects, and enhanced reliability for characterizing CdZnO thin films. The significance of this study lies in improving the existing method and systematizing it for all ternary semiconductors, including thin films, heterostructures, and other related materials.

4.1.2 Summary of Key Findings of Publication I

In this paper, we investigated the use of the calibration curve approach to accurately quantify Cd in $Cd_{1-x}Zn_xO$ thin films, focusing on addressing matrix effects in SIMS analysis. Both MS-SIMS and ToF-SIMS were employed to analyze the samples. The study emphasized improving sensitivity and precision for elemental composition analysis. Key findings and contributions are summarized below:

- We employed the MS-SIMS instrument with a $Cs^{\pm}$ ion beam at 10 keV, optimizing the beam current for secondary ion generation and minimizing sample damage.
- The beam spot size was carefully controlled using an aperture to achieve high spatial resolution while maintaining a stable secondary ion yield, ensuring uniform bombardment across the target areas.
- The primary ion beam was focused using the SIMS optical alignment system, with lens adjustments to optimize beam intensity for effective ionization of the sample surface. Samples were placed in the chamber, and various regions were examined to confirm suitable measurement sites and compositional uniformity.
- To further validate the results, we performed ToF-SIMS, allowing for a comparison with MS-SIMS data and enhancing the sensitivity of the measurements.
- The ion beams (Bi^+ for analysis and Cs^+ for sputtering) were selected with suitable currents to optimize ionization and minimize damage. Rastering areas and optical settings were adjusted to ensure accurate beam focus and alignment for effective depth profiling for this instrument.
- Depth profiling was performed by sputtering the sample with the primary beam while measuring the secondary ion signals. To avoid mass overlap, isotopes of

elements were carefully chosen. After setup optimization, signals for Cd^+, Zn^+, and their molecular clusters ($CdCs^+$, $ZnCs^+$) were collected.

- Calibration curves were constructed by relating Cd compositions determined from EDX measurements with ion signal intensities from SIMS. Ratios of $CdCs^+ / ZnCs^+$ and Cd^+ / Zn^+ were plotted against the Sn-to-Pb mole fraction. Linear fits were used to derive calibration formulas for single ions and molecular clusters individually.

- Our results confirmed using molecular ion signals (MCs^+) provided a more accurate representation of Cd composition by mitigating matrix effects. These signals aligned well with established literature, validating the approach.

- The MS-SIMS signal for MCs^+ resulted in a more reliable calibration curve than ToF-SIMS due to the stronger ion signal and improved sensitivity in MS-SIMS from differences in primary beam currents.

- The study highlighted the shortcomings of traditional quantification methods (e.g., RSF) for higher $x > 1\%$ content and demonstrated that the calibration curve approach offers superior accuracy for ternary semiconductors, where precise quantification of matrix composition is critical for material properties.

This research establishes the calibration curve as a reliable method for addressing matrix effects in SIMS, enhancing accuracy and sensitivity for characterizing ternary compounds like $Cd_{1-x}Zn_xO$. These advances are crucial for applications in materials science and semiconductor technology.

4.2 Quantification of PbSnTe

4.2.1 Summary of Key Findings of Publication II:

In this paper, we investigated the matrix effects in SIMS analysis, focusing on their influence on the quantification of the ternary compound $Pb_{1-x}Sn_xTe$. The study aimed to establish a robust calibration method for accurately determining the elemental composition of $Pb_{1-x}Sn_xTe$ thin films, addressing the challenges posed by non-linear ion yield variations due to matrix effects. The MS-SIMS instrument was employed to analyze the sample composition. The key contributions and findings of this work are summarized below:

- $Cs^{\pm}$ primary ion beam was utilized at 10 keV to optimize secondary ion generation for the ternary compound $Pb_{1-x}Sn_xTe$. The beam current was precisely adjusted to balance sensitivity with minimal sample damage, ensuring reliable and reproducible data acquisition.

- An optimized aperture was selected to define the beam spot size, providing high spatial resolution while maintaining a consistent secondary ion yield. This adjustment was critical to achieving precise and uniform bombardment across the analyzed areas.

- The SIMS optical alignment system was used to focus the primary ion beam meticulously. Fine adjustments to the lens system ensured a tightly focused beam with enhanced intensity, enabling high-quality ionization of the sample surface.

- Samples were systematically placed in the analysis chamber, and the primary beam was directed at different regions to identify appropriate measurement sites and verify compositional uniformity.

- The isotopes of elements were carefully selected for the SIMS measurement to avoid mass overlapping, ensuring comprehensive data collection and enabling using a single detector. After optimizing the setup, signals for $Pb^{\pm}$, $Sn^{\pm}$, and their molecular clusters with Cs ($PbCs^{+}$ and $SnCs^{+}$) were acquired for analysis.

- To correlate the sputtering time with the depth of the profile, we used a DEKTAK 6M stylus profiler to measure the crater's depth. The x-axis of the depth profile,

corresponding to the sputtering time, was converted to depth for each sample. This step was essential for establishing an accurate depth profile for calibration purposes.

- Calibration curves were constructed using the known Sn compositions in each sample as measured by EDX and the SIMS measured ion signal intensities. Signal ratios of $SnCs^+/PbCs^+$ and $Sn^\pm/Pb^\pm$ were calculated and plotted against the Sn to Pb mole fraction. A linear function was fitted to these experimental data points to derive calibration formulas for both single ions (positive and negative) and their molecular clusters.

- The developed calibration formulas effectively correlated the SIMS signal intensities to the elemental composition of $Pb_{1-x}Sn_xTe$, mitigating matrix effects and providing a reliable method for quantifying ternary compounds.

This study significantly enhances the reliability of SIMS for material characterization, overcoming limitations associated with variable ion yields caused by matrix composition. These advancements offer profound implications for applications in materials science, electronics, and semiconductor technology, enhancing the precision and applicability of SIMS in analyzing complex materials.

4.2.2 Summary of Key Findings of Publication III:

This research investigates how electronic properties of material affect ionization yields and matrix effects in SIMS analysis of the ternary compound $Pb_{1-x}Sn_xTe$, with a focus on understanding the relationship between composition and secondary ion behavior and its relation with changes in the work function (ϕ) and electron affinity of the material (A_m). The primary contributions of this work are as follows:

- We optimized the $Cs^{\pm}$ primary ion beam at 10 keV for each series of samples to maximize secondary ion generation while minimizing sample damage. The beam current, aperture size, and beam focus were carefully tuned to achieve high spatial resolution and reliable data collection.

- The first series of samples, consisting of homogeneous materials with varying Sn content from sample to sample, was bombarded to collect the signal of $Pb^{\pm}$, $Sn^{\pm}$, and $Te^{\pm}$ for depth profiling analysis. The isotopes of the detected elements were carefully selected to prevent mass overlap, and all signals were acquired using a single detector to ensure accurate data collection.

- For the second series of graded samples, where Sn content varied with depth, energy distribution profiles were measured. We estimated the Sn content in these samples using the calibration formula from our previous study, showing good agreement with MBE-designed profiles.

- The samples were mounted in the chamber, and sputtering was performed with the sample potential varied to collect energy distribution data for both positive and negative secondary ions.

- A unique aspect of this study was manually adjusting the sample voltage to monitor energy profile shifts. Despite a device limitation of 0.16 eV energy resolution, careful monitoring of depth profiles ensured accurate measurement of ionization behavior and energy distribution shifts as Sn content varied. These shifts were linked to the work function for negative ions and the electron affinity of materials for positive ions, providing valuable insight into the electronic properties of $Pb_{1-x}Sn_xTe$.

- A breaking point was observed in the SIMS signal ratio, which corresponded to the band gap crossing point, highlighting a novel application of SIMS to monitor the electronic properties of ternary semiconductors.

- For the first time, we demonstrated that discontinuities in ϕ and A_m and, as a result, in SIMS signal ratios, are linked to the behavior of valence and conduction bands

in $Pb_{1-x}Sn_xTe$, specifically the changes in Sn content. This led to the proposal of a band offset model, which can estimate the electronic properties of $Pb_{1-x}Sn_xTe$ as a function of Sn content.

- This study is the first to establish a connection between ionization probabilities and electronic properties in ternary semiconductors, specifically regarding work function and electron affinity. These findings are significant for evaluating the band structure and behavior of topological crystalline insulators and provide a model for predicting the electronic properties of ternary compounds based on Sn content.

The work demonstrates the potential of SIMS for observing band gap behavior and ionization dynamics in ternary semiconductor materials, contributing new insights into the application of SIMS for material characterization and the study of electronic properties in advanced materials. More importantly, a new application for SIMS.

4.3 Publications:

Publication I

Authorship Statement

I declare that I am the co-author of the publication:

Accurate determination of matrix composition in $Cd_{1-x}Zn_xO$ semiconductor material using MS-SIMS and ToF-SIMS methods.
Khosravizadeh, Z., Trzyna-Sowa, M., Lysak, A., Przeździecka, E., Jakiela, R.
Journal of Physics D: Applied Physics, 58 (2024) 025303.
http://iopscience.iop.org/article/10.1088/1361-6463/ad80a0

I contributed equally to the conceptualization. I took the lead role in data curation, analysis, investigation, methodology, validation, and visualization. I was responsible for the original writing and contributed equally to the review and editing process.

Signature: 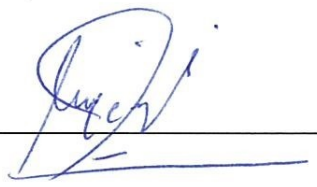

Date: 10.12.2024

Uniwersytet Rzeszowski
Kolegium Nauk Przyrodniczych
Instytut Inżynierii Materiałowej
Centrum Dydaktyczno-Naukowe Mikroelektroniki i Nanotechnologii

STATEMENT

I declare that I am the co-author of the publication:

Accurate determination of matrix composition in $Cd_{1-x}Zn_xO$ semiconductor material using MS-SIMS and ToF-SIMS methods.
Khosravizadeh, Z., Trzyna-Sowa, M., Lysak, A., Przezdziecka, E., Jakiela, R.
Journal of Physics D: Applied Physics, 19(4): 041019-041028, 2024.
http://iopscience.iop.org/article/10.1088/1361-6463/ad80a0

I contributed to TOF-SIMS measurement.

Signature: Małgorzata Trzyna-Sowa

Date: 29. 11. 2024

ul. prof. Stanisława Pigonia 1, 35-310 Rzeszów
tel.: +48 17 851 86 70
e-mail: cmikroinano@ur.edu.pl

AUTHORSHIP STATEMENT

I declare that I am the co-author of the publications:

- Accurate determination of matrix composition in $Cd_{1-x}Zn_xO$ semiconductor material using MS-SIMS and ToF-SIMS methods – Khosravizadeh, Z., Trzyna-Sowa, M., Lysak, A., Przezdziecka, E., Jakiela, R. Journal of Physics D: Applied Physics, 19(4) (2024) 041019, DOI /10.1088/1361-6463/ad80a0

I contributed to the growth of the samples using the MBE method and EDX measurements.

Signature: Anastasiia Lysak

Date: 5-12-2024

AUTHORSHIP STATEMENT

I declare that I am the co-author of the publications:

- Accurate determination of matrix composition in $Cd_{1-x}Zn_xO$ semiconductor material using MS-SIMS and ToF-SIMS methods – Khosravizadeh, Z., Trzyna-Sowa, M., Lysak, A., Przezdziecka, E., Jakiela, R. Journal of Physics D: Applied Physics, 19(4) (2024) 041019, DOI /10.1088/1361-6463/ad80a0

I contributed to the planning and development of sample growth parameters and sample growth using the MBE method, as well as discussed some of the results.

Signature: Ewa Przeździecka

Date: 09.12.24

AUTHORSHIP STATEMENT

I declare that I am the co-author of the publications:

- Accurate determination of matrix composition in $Cd_{1-x}Zn_xO$ semiconductor material using MS-SIMS and ToF-SIMS methods – Khosravizadeh, Z., Trzyna-Sowa, M., Lysak, A., Przezdziecka, E., Jakiela, R. Journal of Physics D: Applied Physics, 19(4) (2024) 041019, DOI /10.1088/1361-6463/ad80a0

I contributed to the substantive supervising of the publication

Signature: 

Date: 10/12/2024

Publication II

Authorship Statement

I declare that I am the co-author of the publication:

Secondary Ion Mass Spectrometry Characterization of Matrix Composition in Topological Crystalline Insulator $Pb_{1-x}Sn_xTe$.
Khosravizadeh, Z., Dziawa, P., Dad, S., Jakiela, R.
Thin Solid Films, 781 (2023) 139974
https://doi.org/10.1016/j.tsf.2023.139974

I contributed equally to the conceptualization. I took the lead role in data curation, analysis, investigation, methodology, validation, and visualization. I was responsible for the original writing and contributed equally to the review and editing process.

Signature: 

Date: 10.12.2024

Authorship Statement

I declare that I am the co-author of the publication:

Secondary Ion Mass Spectrometry Characterization of Matrix Composition in Topological Crystalline Insulator $Pb_{1-x}Sn_xTe$.
Khosravizadeh, Z., Dziawa, P., Dad, S., Jakiela, R.
Thin Solid Films, 781 (2023) 139974
https://doi.org/10.1016/j.tsf.2023.139974

My contribution to the work, including the MBE growth of the studied samples and EDX measurements.

Signature: Piotr Dziawa

Date: 06.12.2024

Authorship Statement

I declare that I am the co-author of the publication:

Secondary Ion Mass Spectrometry Characterization of Matrix Composition in Topological Crystalline Insulator $Pb_{1-x}Sn_xTe$.
Khosravizadeh, Z., Dziawa, P., Dad, S., Jakiela, R.
Thin Solid Films, 781 (2023) 139974
DOI: https://doi.org/10.1016/j.tsf.2023.139974

I contributed to the Molecular Beam Epitaxial growth of the studied samples and EDX measurements.

Signature: Zaviadadeh

Date: 05/12/2024

AUTHORSHIP STATEMENT

I declare that I am the co-author of the publications:

- Secondary Ion Mass Spectrometry Characterization of Matrix Composition in Topological Crystalline Insulator $Pb_{1-x}Sn_xTe$ – Khosravizadeh, Z., Dziawa, P., Dad, S., Jakiela, R., Thin Solid Films, 781 (2023) 139974, DOI /10.1016/j.tsf.2023.139974.

I contributed to the substantive supervising of the publication

Signature: 

Date: 10/12/2024

Publication III

Authorship Statement

I declare that I am the co-author of the publication:

A novel approach for observing band gap crossings using the SIMS technique in $Pb_{1-x}Sn_xTe$.
Khosravizadeh, Z., Dziawa, P., Dad, S., Dabrowski, A., Jakiela, R.
Journal of Semiconductors, 45 (2024) 112102.
https://www.jos.ac.cn/en/article/doi/10.1088/1674-4926/24040023

I contributed equally to the conceptualization. I took the lead role in data curation, analysis, investigation, methodology, validation, and visualization. I was responsible for the original writing and contributed equally to the review and editing process.

Signature: _____

Date: 10.12.2024

Authorship Statement

I declare that I am the co-author of the publication:

A novel approach for observing band gap crossings using the SIMS technique in $Pb_{1-x}Sn_xTe$.
Khosravizadeh, Z., Dziawa, P., Dad, S., Dabrowski, A., Jakiela, R.
Journal of Semiconductors, 45 (2024) 112102.
https://www.jos.ac.cn/en/article/doi/10.1088/1674-4926/24040023

My contribution to the work, including the MBE growth of the studied samples and the reviewing and editing the draft.

Signature: Piotr Dziawa

Date: 06.12.2024

Authorship Statement

I declare that I am the co-author of the publication:

A novel approach for observing band gap crossings using the SIMS technique in $Pb_{1-x}Sn_xTe$.
Khosravizadeh, Z., Dziawa, P., Dad, S., Dabrowski, A., Jakiela, R.
Journal of Semiconductors, 45 (2024) 112102.
DOI: 10.1088/1674-4926/24040023

I contributed to the Molecular Beam Epitaxial growth of studied samples and Hall measurements.

Signature: Semiadak

Date: 05/12/2024

STATEMENT

I declare that I am the co-author of the publication:

A novel approach for observing band gap crossings using the SIMS technique in $Pb_{1-x}Sn_xTe$.
Khosravizadeh, Z., Dziawa, P., Dad, S., Dabrowski, A., Jakiela, R.
Journal of Semiconductors, 45(11): 112102, 2024.
https://www.jos.ac.cn/en/article/doi/10.1088/1674-4926/24040023

I contributed to preparation and conduct of Hall measurement

Signature: _____

Date: 28.11.2024

AUTHORSHIP STATEMENT

I declare that I am the co-author of the publications:

- A novel approach for observing band gap crossings using the SIMS technique in $Pb_{1-x}Sn_xTe$ – Khosravizadeh, Z., Dziawa, P., Dad, S., Dabrowski, A., Jakiela, R., Journal of Semiconductors, 45 (2024) 112102, DOI /10.1088/1674-4926/24040023.

I contributed to the substantive supervising of the publication

Signature: 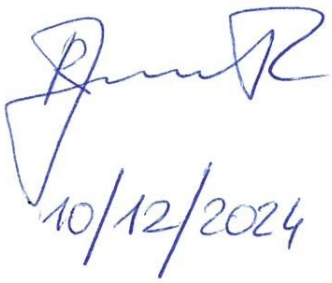

Date: 10/12/2024

Chapter 5

Conclusions and Outlook

5.1 Addressing the Research Questions

This thesis investigated matrix effects in the SIMS method for analyzing ternary semiconductors, addressing challenges in precise elemental quantification and advancing electronic property characterization. The research focused on answering three core questions, each of which is addressed through the results presented below:

RQ 1: *How do matrix effects impact SIMS measurement accuracy?*

Matrix effects significantly influence SIMS measurements by altering the ionization probabilities of atoms during sputtering. This study demonstrated that in ternary semiconductors such as CdZnO and PbSnTe, variations in secondary ion yields stem from differences in electronic properties, elemental ratios, and chemical bonding. These effects are particularly pronounced in complex structures like heterostructures and superlattices, creating challenges for interpreting raw SIMS data. Without proper calibration, these matrix effects introduce uncertainty into composition measurements.

RQ 2: *How can we overcome matrix effects for precise quantification in SIMS?*

To overcome matrix effects, this research developed and validated novel calibration curves tailored to CdZnO and PbSnTe. These calibration curves provided an accurate method for quantifying elemental content using SIMS signal ratios of matrix elements. Key advancements include:

- Calibration curves reliably determined unknown compositions in ternary semiconductor structures.
- The MCs^+ cluster approach effectively mitigated matrix effects, improving measurement precision in complex thin films.
- Comparative analysis revealed that while the RSF method is effective for low-content elements (namely dopants), the calibration curve approach is more accurate for high-content elements (namely matrix elements).

RQ 3: *What is the role of electronic properties of ternary semiconductors in matrix effects?*

The research established a critical link between electronic properties—such as work function and electron affinity—and the manifestation of matrix effects in SIMS. For PbSnTe, variations in secondary ion yields correlated with shifts in the energy distribution of emitted ions. These changes were linked to electronic properties and band gap behavior. Highlights include:

- Significant changes in SIMS signal ratios near the critical band crossing point corresponded to the valence band maximum (VBM) and conduction band minimum (CBM) evolution.
- The study predicted band gap behavior by analyzing ionization probabilities and shifts in secondary ions' energy distribution. This is a novel application for electronic property characterization of ternary semiconductors using the SIMS method.

5.2 General Conclusions

By addressing these research questions, this thesis highlights the transformative potential of SIMS in material characterization by addressing challenges associated with matrix effects and achieving precise elemental quantification in ternary semiconductors. It is important to note that even minor differences in estimating the composition of materials can significantly impact their electrical and optical properties. The precise quantification of matrix composition in ternary compound semiconductors is necessary due to the development of advanced semiconductor technology. Combining innovative calibration techniques with insights into electronic properties, the study significantly advances the understanding and application of SIMS for complex materials.

The main results are summarized as follows:

- A novel approach was developed and improved to create calibration curves by analyzing the SIMS signal ratio of matrix elements in CdZnO and PbSnTe.
- Calibration curves were essential in constructing a formula to calculate unknown amounts of compositions in PbSnTe and CdZnO across varied structures like heterostructures or superlattices, dramatically increasing the accuracy of material analysis.
- The MCs^+ clusters reduced deviations from ideal calibration curves compared to single ions, effectively mitigating matrix effects and enabling more accurate content determination in complex thin films.

- The study revealed a new application of SIMS in evaluating the energy band gap behavior in ternary compound semiconductors, particularly for $Pb_{1-x}Sn_xTe$ compound with band crossings in its electronic structure.
- By analyzing ionization probabilities and energy distribution shifts of secondary ions and linking them to electronic properties such as work function and electron affinity, this work successfully predicted the band gap behavior of $Pb_{1-x}Sn_xTe$ for the first time by SIMS.
- The evolution of the VBM and CBM as the Sn composition varied from 0 (pure PbTe) to 1 (pure SnTe) was observed, with critical changes in SIMS signal ratios linked to the band crossing position in $Pb_{1-x}Sn_xTe$.
- A comparative analysis between the RSF method and the calibration curve approach in $Cd_{1-x}Zn_xO$ thin films demonstrated that RSF is reliable for low-content elements, but the calibration curve method is much more precise for higher-content elements.
- Discrepancies between calibration curves derived from MS-SIMS and ToF-SIMS instruments were attributed to differences in analyzing beams affecting secondary ion signals. This finding highlights the importance of selecting appropriate techniques for material characterization.

This thesis demonstrated the effectiveness of advanced material characterization techniques, such as SIMS, in accurately quantifying the matrix elements by reducing the impact of the matrix effects. It provides a foundation for applying these techniques to a broader range of materials.

5.3 Outlook

The findings emphasize the importance of accurate composition quantification in ternary compounds for advanced semiconductor devices. While this study focused on CdZnO and PbSnTe, the methodologies and insights can be extended to other ternary and quaternary systems. Future research should focus on:

- Investigating calibration curves for wide band-gap ternary compounds such as MgZnO or AlGaN.
- Studying ternary compounds combining narrow and wide band-gap semiconductors, such as AlInN, to enhance understanding of composition impacts on energy distribution profiles.

- Exploring topological materials with magnetic properties, such as PbSnTe(: Cr: Mn), using SIMS to compare its electronic properties behavior with our results.
- Assessing how matrix effects influence dopant quantification and diffusion characterization, particularly for elements like Cr and Mn in PbSnTe and impurities like H and C in CdZnO.
- Estimation of the dependency of the elemental RSF on the ternary compound composition (RSF calibration curve).
- Continuing research to enhance material performance and achieve precise control over thin-film characteristics, contributing to advancements in applications such as next-generation electronic devices.

This thesis paves the way for future advancements in semiconductor technology, emphasizing the role of precise material characterization in enabling innovative applications.

Bibliography

[1] A. Yamaguchi, Material characterization of semiconductor devices, SEI Technical Review 70 (2010) 2. doi:https://sumitomoelectric.com/sites/default/files/2020-12/download_documents/70-02.pdf.

[2] K. Miyoshi, Surface characterization techniques: An overview, Tech. Rep. NASA/TM-2002-211497, NASA Glenn Research Center, Cleveland, OH, United States (2002). doi:20020070606.pdf.

[3] M. Pech-Canul, N. Ravindra, Semiconductors: synthesis, properties and applications, 1st Edition, Springer, 2019. doi:10.1007/978-3-030-02171-9.

[4] C. A. Evans, R. Brundle, S. Wilson, Encyclopedia of Materials Characterization: Surfaces, Interfaces, Thin Films, 1st Edition, Butterworth-Heinemann, 1992. doi:10.1016/C2009-0-26077-6.

[5] R. Wilson, F. Stevie, C. Magee, Secondary ion mass spectrometry: a practical handbook for depth profiling and bulk impurity analysis, Wiley-Interscience, 1989. doi:https://api.semanticscholar.org/CorpusID:136128655.

[6] G. McGuire, Characterization of semiconductor materials, Vol. Volume 1, Noyas Publications, Mill Road, Park Ridge, New Jersey, United States, 1989. doi:https://www.academia.edu/9558362/CHARACTERIZATION_OF_SEMICONDUCTOR_MATERIALS_Principles_and_Methods_Volume_I_Edited_by.

[7] H. Werner, Secondary ion mass spectrometry and its application in thin film and surface layer research, Jpn. J. Appl. Phys. 13 (1974) 367. doi:10.7567/JJAPS.2S1.367.

[8] A. Benninghoven, F. Rudenauer, H. Werner, Secondary ion mass spectrometry: basic concepts, instrumental aspects, applications and trends, John Wiley and Sons, New York, 1987. doi:https://www.osti.gov/biblio/6092161.

[9] V. Deline, W. Katz, C. Evans Jr, P. Williams, Mechanism of the SIMS matrix effect, Appl. Phys. Lett. 33 (1978) 832–835. doi:https://doi.org/10.1063/1.90546.

[10] G. Siddharth, R. Singh, V. Garg, B. Sengar, M. Das, B. Mandal, M. Htay, M. Gupta, S. Mukherjee, Investigation of dibs-deposited CdZnO/ZnO-based multiple quantum well for large-area photovoltaic application, IEEE Trans. Electron Devices 67 (2020) 5587–5592. doi:10.1109/TED.2020.3031235.

[11] N. Moussa, F. Ebrahim, K. Adly, M. Hassaan, Chromium doped ZnO nanoparticles for energy storage, gas and humidity sensing and spin based electronic devices applications, Opt. Quant Electron. 54 (2022) 683. doi:https://doi.org/10.1007/s11082-022-04075-y.

[12] M. Pietrzyk, A. Wierzbicka, E. Zielony, A. Pieniazek, R. Szymon, E. Placzek-Popko, Fundamental studies of ZnO nanowires with ZnCdO/ZnO multiple quantum wells grown for tunable light emitters, Sens. Actuators A: Phys. 315 (2020) 112305. doi:https://doi.org/10.1016/j.sna.2020.112305.

[13] Q. Wang, J. Li, Y. Lei, Y. Wen, Z. Wang, X. Zhan, F. Wang, F. Wang, Y. Huang, K. Xu, J. He, Oriented growth of $Pb_{1-x}Sn_xTe$ nanowire arrays for integration of flexible infrared detectors, Adv. Mater. 28 (2016) 3596–3601. doi:https://doi.org/10.1002/adma.201506338.

[14] J. Walpole, A. Calawa, T. Harman, S. Groves, Double-heterostructure PbSnTe lasers grown by molecular-beam epitaxy with cw operation up to 114 K, Appl. Phys. Lett. 28 (1976) 552–554. doi:https://doi.org/10.1063/1.88820.

[15] M. Yoshikawa, K. Shinohara, R. Ueda, Continuous operation over 1500 h of a PbTe/PbSnTe double-heterostructure laser at 77 k, Applied Physics Letters 31 (1977) 699–701. doi:https://doi.org/10.1063/1.89491.

[16] J. Donnelly, A. Calawa, T. Harman, A. Foyt, W. Lindley, $Pb_{1-x}Sn_xTe$ photovoltaic diodes and diode lasers produced by proton bombardment, Solid-State Electron. 15 (1972) 403–407. doi:https://doi.org/10.1016/0038-1101(72)90111-6.

[17] L. Fu, Topological crystalline insulators, Phys. Rev. Lett. 106 (2011) 106802. doi:https://doi.org/10.1103/PhysRevLett.106.106802.

[18] A. Tarasov, V. Golyashov, D. Ishchenko, I. Akhundov, A. Klimov, V. Epov, A. Kaveev, S. Suprun, V. Sherstyakova, O. Tereshchenko, Field effect and spin-valve effect in the PbSnTe topological crystalline insulator, Optoelectron. Instrum. Data Process. 56 (2020) 553–557. doi:https://doi.org/10.3103/S8756699020050131.

[19] Y. Gao, A new secondary ion mass spectrometry technique for III-V semiconductor compounds using the molecular ions CsM+, J. Appl. Phys. 64 (1988) 3760–3762. doi:https://doi.org/10.1063/1.341381.

[20] H. Gnaser, H. Oechsner, SIMS depth profile analysis using MCs+ molecular ions, Fresenius J. Anal. Chem. 341 (1991) 54–56. doi:https://doi.org/10.1007/BF00322106.

[21] L. Wang, A. Wang, S. Price, Accurate determination of the matrix composition profile of $Hg_{1-x}Cd_xTe$ by secondary ion mass spectrometry, J. Electron. Mater. 36 (2007) 910–912. doi:https://doi.org/10.1007/s11664-007-0131-7.

[22] J. Thomson, LXXXIII. rays of positive electricity, The London, Edinburgh, and Dublin Philosophical Magazine and J. Sci. 20 (1910) 752–767. doi:10.1080/14786441008636962.

[23] R. Herzog, F. Viehböck, Ion source for mass spectrography, Phys. Rev. 76 (1949) 855. doi:https://doi.org/10.1103/PhysRev.76.855.

[24] R. Herzog, W. Poschenrieder, F. Satkiewicz, Mass spectrometer analysis of solid materials with the ion-microprobe sputter source, Tech. rep., GCA CORPORATION Bedford, Mass., no. NAS 5-9254 (1967). doi:https://ntrs.nasa.gov/api/citations/19670005598/downloads/19670005598.pdf.

[25] A. Benninghoven, Surface investigation of solids by the statical method of secondary ion mass spectroscopy (SIMS), Surf. Sci. 35 (1973) 427–457. doi:https://doi.org/10.1016/0039-6028(73)90232-X.

[26] A. Benninghoven, Development in secondary ion mass spectroscopy and applications to surface studies, Surf. Sci. 53 (1975) 596–625. doi:https://doi.org/10.1016/0039-6028(75)90158-2.

[27] H. Werner, A. Torrisi, Interface and thin film analysis: Comparison of methods, trends, Fresenius J Anal Chem 337 (1990) 594–613. doi:https://doi.org/10.1007/BF00323094.

[28] H. Gnaser, Improved quantification in secondary-ion mass spectrometry detecting MCs+ molecular ions, J. Vac. Sci. Technol. A 12 (1994) 452–456. doi:https://doi.org/10.1116/1.579262.

[29] P. Williams, Secondary ion mass spectrometry, Annu. Rev. Mater. Sci. 15 (1985) 517–548. doi:https://doi.org/10.1146/annurev.ms.15.080185.002505.

[30] L. Van Vaeck, A. Adriaens, R. Gijbels, Static secondary ion mass spectrometry (S-SIMS) part 1: methodology and structural interpretation, Mass Spectrom. Rev. 18 (1999) 1–47. doi:https://doi.org/10.1002/(SICI)1098-2787(1999)18:1<1::AID-MAS1>3.0.CO;2-W.

[31] J. Bacon, J. Greenwood, L. Van Vaeck, J. Williams, Atomic spectrometry update. atomic mass spectrometry, J. Anal. At. Spectrom. 18 (2003) 955–997. doi:https://doi.org/10.1039/B306545F.

[32] J. E. Baker, Secondary Ion Mass Spectrometry, Springer New York, New York, NY, 2014, Ch. 4, pp. 133–187. doi:10.1007/978-1-4614-9281-8_4.

[33] EAG Laboratories, SIMS tutorial: Secondary ion mass spectrometry (SIMS), https://www.eag.com/app-note/sims-tutorial/ (2015).

[34] Surface and Interface Laboratory, Rice University, Time of flight secondary ion mass spectrometry (ToF-SIMS), https://simslab.rice.edu/surface-analysis-lab/teaching-activities-resources/time-of-flight-secondary-ion-mass-spectrometry/ (2023).

[35] M. Verruno, Investigation of the enhancement of the performance of the SIMS instruments, Phd thesis, Université Paris-Saclay (2017).

[36] Y. Liang, High-resolution backside SIMS depth profiling, Phd thesis, National University of Singapore (2004).

[37] C. Andersen, Progress in analytic methods for the ion microprobe mass analyzer, Int. J. Mass Spectrom. Ion Phys. 2 (1969) 61–74. doi:https://doi.org/10.1016/0020-7381(69)80006-9.

[38] W. Grove, XXXIII. on some anomalous cases of electrical decomposition, The London, Edinburgh, and Dublin Philosophical Magazine and J. Sci. 5 (1853) 203–209. doi:https://doi.org/10.1080/14786445308647227.

[39] E. Goldstein, The canal-ray group, Verh. Dtsch. Phys. Ges 4 (1902) 228–237.

[40] F. Penning, J. Moubis, Cathode sputtering in a magnetic field, Proceedings, Koninklijke Nederlandsche Akademie van Wetenschappen te Amsterdam 43 (1940) 41–56. doi:https://lib.ugent.be/catalog/rug01:002327558.

[41] A. Güntherschulze, Loss of electrons by collisions with positive ions at low gas pressures, Z. Phys 62 (1930) 600–6.

[42] M. Irvine, Sputtering of an aluminum cathode in a glow discharge maintained in a residual atmosphere of argon, Lehigh University, 1955.

[43] A. Von Hippel, Theory of cathode scattering, Ann. Phys. 386 (1926) 1043.

[44] K. Kingdon, I. Langmuir, The removal of thorium from the surface of a thoriated tungsten filament by positive ion bombardment, Phys. Rev. 22 (1923) 148. doi:https://doi.org/10.1103/PhysRev.22.148.

[45] R. Seeliger, K. Sommermeyer, Bemerkung zur theorie der kathodenzerstäubung, Zeitschrift für Physik 93 (1935) 692–695. doi:https://doi.org/10.1007/BF01330543.

[46] J. Stark, Die elektrizität in gasen, JA Barth, 1902.

[47] G. Wehner, Controlled sputtering of metals by low-energy hg ions, Phys. Rev. 102 (1956) 690. doi:https://doi.org/10.1103/PhysRev.102.690.

[48] E. Lamar, K. Compton, A special theory of cathode sputtering, Science 80 (1934) 541.

[49] F. Keywell, Measurements and collision—radiation damage theory of high-vacuum sputtering, Phys. Rev. 97 (1955) 1611. doi:https://doi.org/10.1103/PhysRev.97.1611.

[50] P. Sigmund, Sputtering by ion bombardment theoretical concepts, Springer Berlin Heidelberg, Berlin, Heidelberg, 1981, pp. 9–71. doi:https://doi.org/10.1007/3540105212_7.

[51] J. Grimblot, M. Abon, Secondary Ion Mass Spectrometry, Springer US, Boston, MA, 1994, Ch. 11, pp. 291–319. doi:10.1007/978-1-4757-9589-9_11.

[52] F. López Fernández, Secondary ion mass spectrometry (sims): principles and applications, https://diposit.ub.edu/dspace/bitstream/2445/32165/1/MT10%20-%20Secondary%20Ion%20Mass%20Spectrometry_ed2.pdf (2012).

[53] A. Belu, D. Graham, D. Castner, Time-of-flight secondary ion mass spectrometry: techniques and applications for the characterization of biomaterial surfaces, Biomaterials 24 (2003) 3635–3653. doi:https://doi.org/10.1016/S0142-9612(03)00159-5.

[54] P. Sigmund, Theory of sputtering. I. sputtering yield of amorphous and polycrystalline targets, Phys. Rev. 184 (1969) 383. doi:https://doi.org/10.1103/PhysRev.184.383.

[55] M. Yu, N. Lang, Mechanisms of atomic ion emission during sputtering, Nucl. Instrum. Methods Phys. Res. Sec. B 14 (1986) 403–413. doi:https://doi.org/10.1016/0168-583X(86)90135-7.

[56] A. Blandin, A. nourtier and dw hone, J. Phys.(Paris) 37 (1976) 369.

[57] R. Brako, D. Newns, Charge exchange in atom-surface scattering: Thermal versus quantum mechanical non-adiabaticity, Surf. Sci. 108 (1981) 253–270. doi:https://doi.org/10.1016/0039-6028(81)90448-9.

[58] M. Yu, N. Lang, Direct evidence of electron tunneling in the ionization of sputtered atoms, Phys. Rev. Lett. 50 (1983) 127–130. doi:10.1103/PhysRevLett.50.127.

[59] V. Deline, C. Evans, P. Williams, A unified explanation for secondary ion yields, Appl. Phys. Lett. 33 (1978) 578–580. doi:https://doi.org/10.1063/1.90466.

[60] K. Wittmaack, Comment on a unified explanation for secondary-ion yields and mechanism of the SIMS matrix effect, J. Appl. Phys. 52 (1981) 527–529. doi:https://doi.org/10.1063/1.328451.

[61] S. Datz, Condensed Matter: Applied Atomic Collision Physics, Vol. 4 of Applied Atomic Collision Physics, Elsevier Science, 2013. doi:https://books.google.pl/books?id=Nrs3BQAAQBAJ.

[62] D. Kumar, A. Patel, Matrix effect, Slideshare.net, presentation on matrix effects in bioanalytical research (2010). doi:https://www.slideshare.net/slideshow/matrix-effect-7614914/7614914.

[63] C. Flynn, Spectroscopy of impurities in metals and on metal surfaces, in: D. J. Fabian, H. Kleinpoppen, L. M. Watson (Eds.), Inner-Shell and X-Ray Physics of Atoms and Solids, Springer US, Boston, MA, 1981, pp. 801–804. doi:10.1007/978-1-4615-9236-5_156.

[64] M. Betti, R. Biagi, U. Pennino, C. Mariani, M. Pedio, Cesium-induced electronic states and space-charge-layer formation in cs/insb(110) interface, Phys. Rev. B 53 (1996) 13605–13612. doi:10.1103/PHYSREVB.53.13605.

[65] P. Williams, The sputtering process and sputtered ion emission, Surf. Sci. 90 (1979) 588–634. doi:https://doi.org/10.1016/0039-6028(79)90363-7.

[66] G. Blaise, M. Bernheim, Adsorption of gases studied by secondary ion emission mass spectrometry, Surf. Sci. 47 (1975) 324–343. doi:https://doi.org/10.1016/0039-6028(75)90298-8.

[67] J. Nørskov, B. Lundqvist, Secondary-ion emission probability in sputtering, Phys. Rev. B 19 (1979). doi:https://doi.org/10.1103/PhysRevB.19.5661.

[68] M. Yu, Charged and excited states of sputtered atoms, Springer Berlin Heidelberg, 1991, Ch. 3, pp. 91–160. doi:10.1007/3540534288$_17$.

[69] W. Monch, Interface states, in: Semiconductor Surfaces and Interfaces, Springer Berlin Heidelberg, Berlin, Heidelberg, 1995, pp. 75–92. doi:10.1007/978-3-662-03134-6_6.

[70] M. Desjonquères, D. Spanjaard, Electronic Structure of Surfaces, Springer Berlin Heidelberg, 1996, Ch. 5, pp. 162–410. doi:https://doi.org/10.1007/978-3-642-61400-2_5.

[71] H. Yamazaki, S. Nakamura, Work-function changes in high-dose B-implanted Si with keV Cs+ bombardment, Phys. Rev. B 59 (1999) 12298–12300. doi:10.1103/PhysRevB.59.12298.

[72] A. Janssen, P. Akhter, C. Harland, J. Venables, High spatial resolution surface potential measurements using secondary electrons, Surf. Sci. 93 (1980) 453–470. doi:https://www.sciencedirect.com/science/article/pii/0039602880902769.

[73] H. Gnaser, Initial stages of cesium incorporation on keV-Cs+-irradiated surfaces: Positive-ion emission and work-function changes, Phys. Rev. B 54 (1996) 17141. doi:https://doi.org/10.1103/PhysRevB.54.17141.

[74] H. Gnaser, Exponential scaling of sputtered negative-ion yields with transient work-function changes on Cs+-bombarded surfaces, Phys. Rev. B 54 (1996) 16456. doi:https://doi.org/10.1103/PhysRevB.54.16456.

[75] D. P. Woodruff, Modern techniques of surface science, Cambridge university press, 2016.

[76] H. Bonzel, Alkali-metal-affected adsorption of molecules on metal surfaces, Surf. Sci. Rep. 8 (1988) 43–125. doi:10.1016/0167-5729(88)90007-6.

[77] G. Blaise, G. Slodzian, Effets comparés de l'oxygène sur l'émission ionique et le potentiel de surface des métaux, Surf. Sci. 40 (1973) 708–714. doi:10.1016/0039-6028(73)90154-4.

[78] N. Lang, Ionization probability of sputtered atoms, Phys. Rev. B 27 (1983) 2019–2029. doi:10.1103/PhysRevB.27.2019.

[79] G. Shao, Work function and electron affinity of semiconductors: Doping effect and complication due to fermi level pinning, Energy Environ. Mater. 4 (2021) 273–276. doi:https://doi.org/10.1002/eem2.12218.

[80] M. Yu, Work-function dependence of negative-ion production during sputtering, Phys. Rev. Lett. 40 (1978) 574. doi:https://doi.org/10.1103/PhysRevLett.40.574.

[81] M. Yu, A comment on the effects of Cs on photon and secondary ion emission during sputtering, Surf. Sci. 90 (1979) 442–446. doi:https://doi.org/10.1016/0039-6028(79)90354-6.

[82] M. Yu, Effect of surface chemistry and work function in secondary ion mass spectrometry, J. Vac. Sci. Technol. A 1 (1983) 500–502. doi:https://doi.org/10.1116/1.571915.

[83] G. Blaise, A. Nourtier, Experimental and theoretical approaches to the ionization process in secondary-ion emission, Surf. Sci. 90 (1979) 495–547. doi:https://doi.org/10.1016/0039-6028(79)90358-3.

[84] C. Andersen, J. Hinthorne, Thermodynamic approach to the quantitative interpretation of sputtered ion mass spectra, Anal. Chem. 45 (1973) 1421–1438. doi:10.1021/ac60330a034.

[85] H. Hantsche, Comparison of basic principles of the surface-specific analytical methods: AES/SAM, ESCA (XPS), SIMS, and ISS with X-ray microanalysis, and some applications in research and industry, Scanning 11 (1989) 257–280. doi:https://doi.org/10.1002/sca.4950110602.

[86] B. Panda, Secondary ion mass spectroscopy (2019). doi:https://ntrs.nasa.gov/api/citations/20190002103/downloads/20190002103.pdf.

[87] V. Gorbenko, Caractérisation par faisceaux d'ions d'hétérostructures III-V pour les applications micro et optoélectroniques, Phd thesis, Université Grenoble Alpes (2006).

[88] R. Hervig, F. Mazdab, P. Williams, Y. Guan, G. Huss, L. Leshin, Useful ion yields for cameca IMS 3f and 6f SIMS: Limits on quantitative analysis, Chemical Geology 227 (2006) 83–99. doi:https://doi.org/10.1016/j.chemgeo.2005.09.008.

[89] A. MacKinnon, Ternary semiconductors, Springer Berlin Heidelberg, Berlin, Heidelberg, 1981, pp. 149–165. doi:10.1007/BFb0108603.

[90] S. M. Sze, K. K. Ng, Physics of Semiconductor Devices, John Wiley & Sons, Inc., Hoboken, NJ, 2006. doi:10.1002/0470068329.

[91] L. Yang, Synthesis and characterization of ZnO nanostructures, Ph.D. thesis, Linköping University Electronic Press (2010).

[92] J. Chu, A. Sher, Physics and properties of narrow gap semiconductors, Springer, 2008. doi:https://doi.org/10.1007/978-0-387-74801-6.

[93] J. Hudgins, Wide and narrow bandgap semiconductors for power electronics: A new valuation, J. Electron. Mater. 32 (2003) 471–477. doi:https://doi.org/10.1007/s11664-003-0128-9.

[94] T. Makino, Y. Segawa, M. Kawasaki, A. Ohtomo, R. Shiroki, K. Tamura, T. Yasuda, H. Koinuma, Band gap engineering based on $Mg_xZn_{1-x}O$ and $Cd_yZn_{1-y}O$ ternary alloy films, Appl. Phys. Lett. 78 (2001) 1237–1239. doi:10.1063/1.1350632.

[95] H. Nanto, T. Minami, S. Shooji, S. Takata, Electrical and optical properties of zinc oxide thin films prepared by rf magnetron sputtering for transparent electrode applications, J. Appl. Phys. 55 (1984) 1029–1034. doi:10.1063/1.333196.

[96] P. Petrou, R. Singh, D. Brodie, The use of ZnO in transparent type MIS solar cells, Appl. Phys. Lett. 35 (1979) 930–931. doi:10.1063/1.91009.

[97] Z. Wang, Zinc oxide nanostructures: growth, properties and applications, J. Phys.: Condens. Matter 16 (2004) R829. doi:10.1088/0953-8984/16/25/R01.

[98] P. Nayar, A. Catalano, Zinc phosphide-zinc oxide heterojunction solar cells, Appl. Phys. Lett. 39 (1981) 105–107. doi:https://doi.org/10.1063/1.92537.

[99] M. Ortega, G. Santana, A. Morales-Acevedo, Optoelectronic properties of CdO/Si photodetectors, Solid-State Electron. 44 (2000) 1765–1769. doi:https://doi.org/10.1016/S0038-1101(00)00123-4.

[100] J. Kocka, C. Konak, The structure of the indirect absorption edge of CdO, Phys. Status Solidi (b) 43 (1971) 731–738. doi:https://doi.org/10.1002/pssb.2220430234.

[101] Y. Choi, C. Lee, S. Cho, Transparent conducting $Zn_xCd_{1-x}O$ thin films prepared by the sol-gel process, TSF 289 (1996) 153–158. doi:https://doi.org/10.1016/S0040-6090(96)08923-7.

[102] K. Sakurai, T. Takagi, T. Kubo, D. Kajita, T. Tanabe, H. Takasu, S. Fujita, S. Fujita, Spatial composition fluctuations in blue-luminescent ZnCdO semiconductor films grown by molecular beam epitaxy, J. Cryst. Growth 237 (2002) 514–517. doi:https://doi.org/10.1016/S0022-0248(01)01954-6.

[103] T. Gruber, C. Kirchner, R. Kling, F. Reuss, A. Waag, F. Bertram, D. Forster, J. Christen, M. Schreck, Optical and structural analysis of ZnCdO layers grown by metalorganic vapor-phase epitaxy, Appl. Phys. Lett. 83 (2003) 3290–3292. doi:10.1063/1.1620674.

[104] S. Shigemori, A. Nakamura, J. Ishihara, T. Aoki, J. Temmyo, $Zn_{1-x}Cd_xO$ film growth using remote plasma-enhanced metalorganic chemical vapor deposition, Jpn. J. Appl. Phys. 43 (2004) L1088. doi:10.1143/JJAP.43.L1088.

[105] A. Ziabari, F. Ghodsi, Optoelectronic studies of sol–gel derived nanostructured CdO–ZnO composite films, J. Alloys Compd. 509 (2011) 8748–8755. doi:https://doi.org/10.1016/j.jallcom.2011.06.050.

[106] A. Huerta-Barberà, E. de Prado, M. Martínez-Tomás, S. Agouram, E. Muñoz, V. Muñoz-Sanjosé, Structural and morphological characterization of the Cd-rich region in $Cd_{1-x}Zn_xO$ thin films grown by atmospheric pressure metal organic chemical vapour deposition, TSF 683 (2019) 128–134. doi:https://doi.org/10.1016/j.tsf.2019.05.044.

[107] M. Martínez-Tomás, A. Huerta-Barberà, S. Agouram, V. Muñoz-Sanjosé, Induced crystallographic changes in $Cd_{1-x}Zn_xO$ films grown on r-sapphire by AP-MOCVD:

the effects of the Zn content when $x \leq 0.5$, CrystEngComm 22 (2020) 74–84. doi:10.1039/C9CE01483G.

[108] X. Fan, H. Sun, Z. Shen, J. Kuo, Y. Lu, A first-principle analysis on the phase stabilities, chemical bonds and band gaps of wurtzite structure $A_xZn_{1-x}O$ alloys (A = Ca, Cd, Mg), J. Phys.: Condens. Matter 20 (2008) 235221. doi:10.1088/0953-8984/20/23/235221.

[109] M. Zahra, A. Ali, A. Khalil, S. Rehman, N. Mushtaq, M. Akbar, R. Raza, Studies of electrical and optical properties of cadmium-doped zinc oxide for energy conversion devices, Fuel Cells 21 (2021) 164–171. doi:https://doi.org/10.1002/fuce.202000026.

[110] C. Bhukkal, R. Vats, B. Goswami, N. Rani, R. Ahlawat, Zinc content (x) induced impact on crystallographic, optoelectronic, and photocatalytic parameters of $Cd_{1-x}Zn_xO$ ($0 \leq x \leq 1$) ternary nanopowder, Mater. Sci. Eng. B 265 (2021) 115001. doi:https://doi.org/10.1016/j.mseb.2020.115001.

[111] W. Mahmoud, A. Al-Ghamdi, Synthesis of CdZnO thin film as a potential candidate for optical switches, Opt. Laser Technol. 42 (2010) 1134–1138. doi:https://doi.org/10.1016/j.optlastec.2010.02.009.

[112] A. Azarov, A. Hallén, B. Svensson, A. Kuznetsov, Annealing of ion implanted CdZnO, J. Phys. D: Appl. Phys. 45 (2012) 235304. doi:10.1088/0022-3727/45/23/235304.

[113] R. Zargar, ZnCdO thick film: a material for energy conversion devices, Mater. Res. Express 6 (2019) 095909. doi:10.1088/2053-1591/ab2fb6.

[114] V. S. Rana, J. K. Rajput, T. K. Pathak, L. Purohit, Porous-shaped n-CdZnO/p-Si heterojunctions for UV photodetectors, Appl. Phys. A 127 (2021) 1–7. doi:https://doi.org/10.1007/s00339-021-04373-4.

[115] R. Zargar, P. Ahmad, M. Gogre, M. Hassan, Screen printing coating of (ZnO) 0.8 (CdO) 0.2 material for optoelectronic applications, Opt. Quant. Electron 52 (2020) 1–12. doi:https://doi.org/10.1007/s11082-020-02511-5.

[116] C. Vieira, D. Soares, M. de Godoy, M. da Silva, L. Vargas, D. Alves, F. Pena, D. Holgado, A. Okazaki, P. Rappl, et al., Heated air sensitivity of $Zn_{1-x}Cd_xO$ films, Mater. Res. Bull. 138 (2021) 111213. doi:https://doi.org/10.1016/j.materresbull.2021.111213.

[117] D. Punetha, S. K. Pandey, CO gas sensor based on E-beam evaporated ZnO, MgZnO, and CdZnO thin films: A comparative study, IEEE Sens. J. 19 (2018) 2450–2457. doi:10.1109/JSEN.2018.2890007.

[118] S. Khayyat, M. Abaker, A. Umar, M. Alkattan, N. Alharbi, S. Baskoutas, Synthesis and characterizations of Cd-doped ZnO multipods for environmental remediation application, J. Nanoscience Nanotechnol. 12 (2012) 8453–8458. doi:10.1166/jnn.2012.6801.

[119] A. Laufer, N. Volbers, S. Eisermann, K. Potzger, S. Geburt, C. Ronning, B. K. Meyer, Determination of secondary ion mass spectrometry relative sensitivity factors for polar and non-polar ZnO, Journal of Applied Physics 110 (9) (2011) 094906. doi:https://doi.org/10.1063/1.3660417.

[120] J. Dimmock, I. Melngailis, A. Strauss, Band structure and laser action in $Pb_xSn_{1-x}Te$, Phys. Rev. Lett. 16 (1966) 1193. doi:10.1103/PhysRevLett.16.1193.

[121] D. Kushev, N. Zheleva, S. Yordanov, The hole effective mass in $Pb_{1-x}Sn_xTe$ near the zero band gap, Phys. Status Solidi (b) 100 (1980) 731–737. doi:10.1002/pssb.2221000242.

[122] S. Ferreira, E. Abramof, P. Motisuke, P. H. O. Rappl, H. Closs, A. Y. Ueta, C. Boschetti, I. N. Bandeira, Experimental observation of band inversion in the PbSnTe system, J. Appl. Phys. 86 (1999) 7198–7200. doi:https://doi.org/10.1063/1.371815.

[123] P. Dziawa, B. Kowalski, K. Dybko, R. Buczko, A. Szczerbakow, M. Szot, E. Łusakowska, T. Balasubramanian, B. M. Wojek, M. H. Berntsen, O. Tjernberg, T. Story, Topological crystalline insulator states in $Pb_{1-x}Sn_xSe$, Nat. Mater. 11 (2012) 1023–1027. doi:https://doi.org/10.1038/nmat3449.

[124] S.-Y. Xu, C. Liu, N. Alidoust, M. Neupane, D. Qian, I. Belopolski, J. Denlinger, Y. Wang, H. Lin, L. a. Wray, et al., Observation of a topological crystalline insulator phase and topological phase transition in $Pb_{1-x}Sn_xTe$, Nat. Commun. 3 (2012) 1192. doi:https://doi.org/10.1038/ncomms2191.

[125] Y. Tanaka, Z. Ren, T. Sato, K. Nakayama, S. Souma, T. Takahashi, K. Segawa, Y. Ando, Experimental realization of a topological crystalline insulator in SnTe, Nat. Phys. 8 (2012) 800–803. doi:https://doi.org/10.1038/nphys2442.

[126] C. Polley, P. Dziawa, A. Reszka, A. Szczerbakow, R. Minikayev, J. Domagala, S. Safaei, P. Kacman, R. Buczko, J. Adell, et al., Observation of topological crystalline insulator surface states on (111)-oriented $Pb_{1-x}Sn_xSe$ films, Phys. Rev. B 89 (2014) 075317. doi:10.1103/PhysRevB.89.075317.

[127] G. Krizman, B. A. Assaf, G. Bauer, G. Springholz, L. A. de Vaulchier, Y. Guldner, Miniband engineering and topological phase transitions in topological-insulator–normal-insulator superlattices, Phys. Rev. B 103 (2021) 235302. doi:https://doi.org/10.1103/PhysRevB.103.235302.

[128] H. Yusheng, A. Grassie, The electronic band structure of $Pb_{1-x}Sn_xTe$ alloys. I. cubic and rhombohedral phase at 4.2 K, J. Phys. F: Met. Phys. 15 (1985) 317. doi:https://doi.org/10.1088/0305-4608/15/2/009.

[129] H. Yusheng, A. D. C. Grassie, The electronic band structure of $Pb_{1-x}Sn_xTe$ alloys. II. temperature dependence through the structural and band inversion transitions, J. Phys. F: Met. Phys. 15 (1985) 337–361. doi:10.1088/0305-4608/15/2/010.

[130] M. Ocio, H. Albany, Two valence band evidence and thermal energy gap in $Pb_{1-x}Sn_xTe$, Phys. Lett. A 27 (1968) 72–73. doi:https://doi.org/10.1016/0375-9601(68)91125-0.

[131] H. Preier, Recent advances in lead-chalcogenide diode lasers, Appl. Phys. 20 (1979) 189–206. doi:10.1007/BF00886018.

[132] S. Ferreira, E. Abramof, P. Motisuke, P. Rappl, H. Closs, A. Ueta, C. Boschetti, I. Bandeira, Band crossing evidence in PbSnTe observed by optical transmission measurements, Brazilian J. Phys. 29 (1999) 771–774. doi:10.1590/S0103-97331999000400033.

[133] I. U. Arachchige, M. G. Kanatzidis, Anomalous band gap evolution from band inversion in $Pb_{1-x}Sn_xTe$ nanocrystals, Nano Lett. 9 (2009) 1583–1587. doi:10.1021/nl8037757.

[134] E. Xu, Z. Li, J. A. Acosta, N. Li, B. Swartzentruber, S. Zheng, N. Sinitsyn, H. Htoon, J. Wang, S. Zhang, Enhanced thermoelectric properties of topological crystalline insulator PbSnTe nanowires grown by vapor transport, Nano Res. 9 (2016) 820–830. doi:https://doi.org/10.1007/s12274-015-0961-1.

[135] Z. Khosravizadeh, P. Dziawa, S. Dad, R. Jakiela, Secondary ion mass spectrometry characterization of matrix composition in topological crystalline insulator $Pb_{1-x}Sn_xTe$, TSF 781 (2023) 139974. doi:10.1016/j.tsf.2023.139974.

[136] Z. Khosravizadeh, P. Dziawa, S. Dad, A. Dabrowski, R. Jakiela, A novel approach for observing band gap crossings using the sims technique in $Pb_{1-x}Sn_xTe$, J. Semicond. 45 (2024) 112102. doi:https://www.jos.ac.cn/en/article/doi/10.1088/1674-4926/24040023.

Institute of Physics, Polish Academy of Sciences

Department of Physics

02-668, Warszawa, Poland

www.ifpan.edu.pl

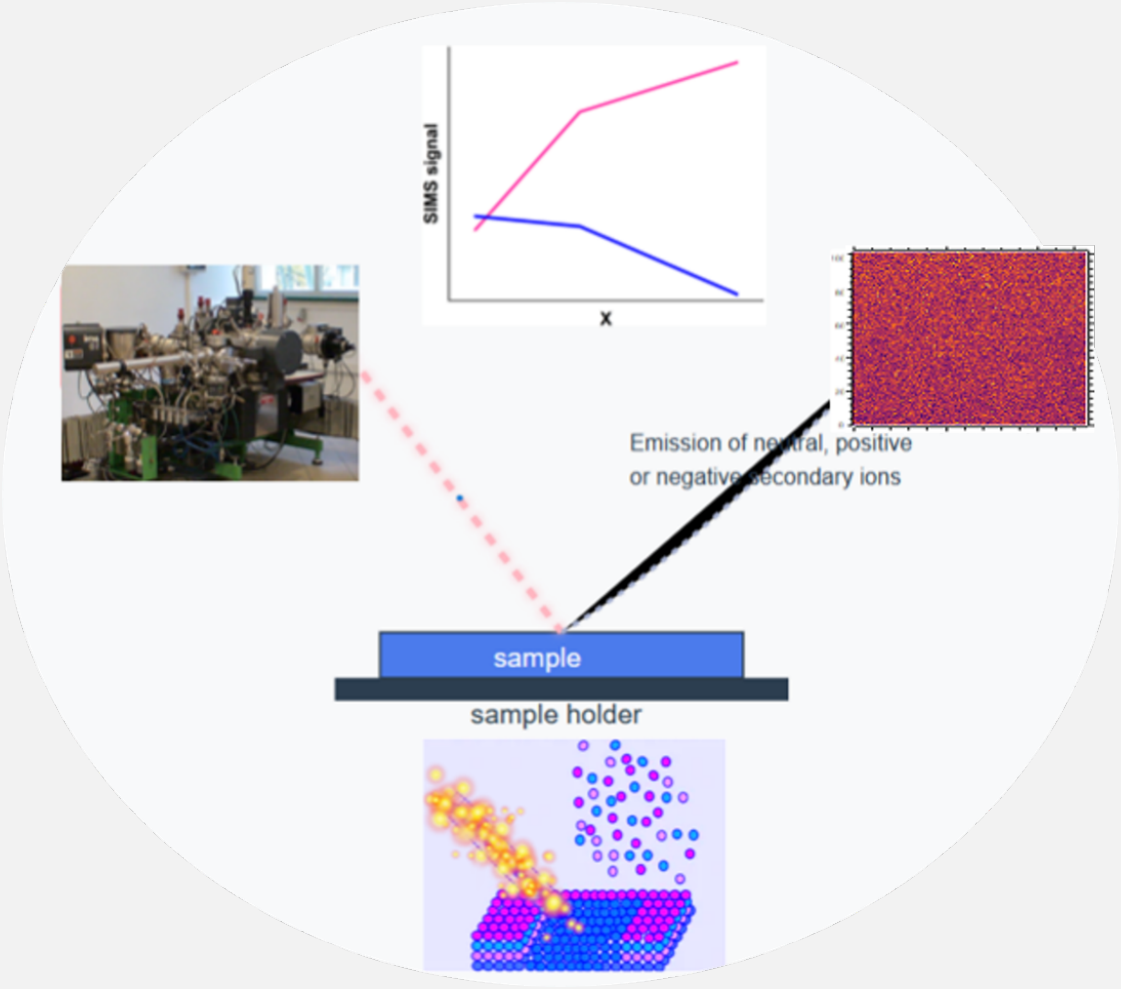

December, 2024

Dostępy do artykułów:

• Khosravizadeh, Z., Trzyna-Sowa, M., Lysak, A., Przeździecka, E., Jakiela, R., “Accurate determination of matrix composition in $Cd_{1-x}Zn_xO$ semiconductor material using MS-SIMS and ToF-SIMS methods,” Journal of Physics D: Applied Physics, 58 (2024) 025303, http://iopscience.iop.org/article/10.1088/1361-6463/ad80a0.

• Khosravizadeh, Z., Dziawa, P., Dad, S., Jakiela, R., “Secondary Ion Mass Spectrometry Characterization of Matrix Composition in Topological Crystalline Insulator $Pb_{1-x}Sn_xTe$,” Thin Solid Films, 781 (2023) 139974, https://doi.org/10.1016/j.tsf.2023.139974.

• Khosravizadeh, Z., Dziawa, P., Dad, S., Dabrowski, A., Jakiela, R., “A novel approach for observing band gap crossings using the SIMS technique in $Pb_{1-x}Sn_xTe$,” Journal of Semiconductors, 45 (2024) 112102, https://www.jos.ac.cn/en/article/doi/10.1088/1674-4926/24040023.